RESEARCH ARTICLES

CHROMOSOMES

Closing the cohesin ring: Structure and function of its Smc3-kleisin interface

Thomas G. Gligoris,[1] Johanna C. Scheinost,[1] Frank Bürmann,[2] Naomi Petela,[1] Kok-Lung Chan,[1,3] Pelin Uluocak,[1,4] Frédéric Beckouët,[1] Stephan Gruber,[2] Kim Nasmyth,[1]* Jan Löwe[5]*

Through their association with a kleisin subunit (Scc1), cohesin's Smc1 and Smc3 subunits are thought to form tripartite rings that mediate sister chromatid cohesion. Unlike the structure of Smc1/Smc3 and Smc1/Scc1 interfaces, that of Smc3/Scc1 is not known. Disconnection of this interface is thought to release cohesin from chromosomes in a process regulated by acetylation. We show here that the N-terminal domain of yeast Scc1 contains two α helices, forming a four-helix bundle with the coiled coil emerging from Smc3's adenosine triphosphatase head. Mutations affecting this interaction compromise cohesin's association with chromosomes. The interface is far from Smc3 residues, whose acetylation prevents cohesin's dissociation from chromosomes. Cohesin complexes holding chromatids together in vivo do indeed have the configuration of hetero-trimeric rings, and sister DNAs are entrapped within these.

A vital member of the Smc/kleisin family is the eukaryotic cohesin complex, which confers sister chromatid cohesion, facilitates the repair of double-strand breaks, and modulates the structure and transcription of interphase chromatin (*1*, *2*). Cohesin contains a dimer of two related Smc proteins, Smc1 and Smc3, whose association with an α-kleisin subunit (Scc1/Rad21) has the potential to form an extended tripartite ring (*3*) within which sister DNAs could be entrapped (*4*). It has been suggested that the cohesin ring has separate DNA entry and exit gates, located at the Smc1/Smc3 "hinge" (*5*) and Smc3/kleisin interfaces, respectively (*6*). To understand how the latter's disconnection by the regulatory subunits Wapl, Pds5, and Scc3 releases cohesin from chromatin and how Smc3 acetylation locks rings shut (*6*), we have determined the structure of the Smc3-kleisin interface.

Structure of the Smc3-Scc1 interface

Because in vivo photo–cross-linking experiments (*7*) showed that Scc1's N-terminal domain (NTD) binds to the coiled coil emerging from Smc3's adenosine triphosphatase (ATPase) head (figs. S1 and S2), we coexpressed in *Escherichia coli* Scc1's first 115 residues (Scc1-N) with a version of the Smc3 ATPase head containing a 75-residue-long section of its coiled coil (Smc3hdCC). This yielded a complex suitable for x-ray crystallography (fig. S2D). Diffraction data were obtained to a resolution of 3.3 Å from crystals grown in the presence of adenosine 5′-*O*-(3-thiotriphosphate) (ATP-γ-S), and their structure was solved by a combination of molecular replacement and selenomethionine (SeMet) single-wavelength anomalous diffraction (SAD) phasing. The structure (Fig. 1A) reveals nearly one third of Smc3's coiled coil, including a pronounced and highly conserved kinked region between L991 and F999 (fig. S3C). The structure of the Smc3 ATPase domain is most closely related to that of Smc1 of all structures currently deposited in the Protein Data Bank (PDB) [root mean square deviation (RMSD) ~ 2.2 Å] (Fig. 1B). (Single-letter abbreviations for the amino acid residues are as follows: A, Ala; C, Cys; D, Asp; E, Glu; F, Phe; G, Gly; H, His; I, Ile; K, Lys; L, Leu; M, Met; N, Asn; P, Pro; Q, Gln; R, Arg; S, Ser; T, Thr; V, Val; W, Trp; and Y, Tyr. In the mutants, other amino acids were substituted at certain locations; for example, L1019R indicates that leucine at position 1019 was replaced by arginine.)

Scc1's NTD is folded into three helices: α1, α2, and α3 (Fig. 1, A and C). The most prominent is the 34-residue α3 (R69-M102), which forms a long helical bundle with Smc3's coiled coil. The C-terminal end of α3 almost reaches the coiled coil's pronounced kink, while the N-terminal end extends to Smc3's ATPase head. Helices α2 and α3 together form a compact four-helix bundle with Smc3's coiled coil, and there is no contact with the ATPase head itself. The very different manner by which N- and C-terminal domains interact with Smc ATPase heads (Fig. 1B) means that the path of Scc1 central domain's polypeptide is complex and possibly influenced by its association with Pds5 and Scc3. Sequences responsible for recruiting Pds5 are situated between H124 and L138 (*7*), close to the top of α3 (Fig. 1D). This proximity is striking because Pds5 has a key role in releasing cohesin from chromatin, presumably by dissociating the Scc1/Smc3 interface, as well as shutting off this process during *S* phase by promoting Smc3K113 acetylation.

Conservation of the Scc1-N/Smc3 interface

The entire surface of Smc3's coiled coil facing Scc1's α3 is highly conserved, whereas the opposing surface is not (Fig. 2A). The face of Scc1's α3 that contacts Smc3's coiled coil is similarly conserved (Fig. 1C and fig. S4, A and D). Scc1's α2 helix is in general less conserved than α3. In a *Bacillus subtilis* complex (*8*), ScpA sequences corresponding to the N-terminal half of Scc1 α3 form a three-helix bundle with the Smc coiled coil similar to that observed between Scc1-N and Smc3, but the structure of the rest of ScpA's NTD differs substantially from that of Scc1 (fig. S4B). Several of the characteristics of α3 are found in β- and γ-kleisins from condensin. Thus, hydrophobic residues such as L75, Y82, L89, and L97, which seem to have a role in contacting Smc3's coiled coils, are present at the same positions within β-kleisins (condensin II) and for the most part also γ-kleisins (condensin I) (fig. S4D). The equivalent residues in *B. subtilis* ScpA are also hydrophobic and have a similar juxtaposition to their Smc partner (*8*).

Testing the structure by use of thiol-specific cross-linking

We created a series of pairwise cysteine substitutions within Scc1 and Smc3 and, using the homo-bifunctional sulfhydryl active reagent dibromobimane (bBBr), measured the efficiency with which these are cross-linked (*9*). Treatment of native cohesin complexes after immunoprecipitation revealed the expected pattern of cross-linking between cysteines within Smc3's coiled coil and cysteines within Scc1's α3 (Fig. 2, B and C). This included cross-linking between Scc1I100C and Smc3F1005C, which confirms that Scc1's α3 extends further up the Smc3 coiled coil than that observed for ScpA (fig. S4B). We also observed efficient cross-linking between Scc1K48C and Smc3K1032C, confirming the observed juxtaposition of α2 with Smc3's coiled coil. In contrast, cross-linking occurred rarely if at all between residues predicted to be nonadjacent (fig S4E). Cysteine pairs involving α2 and α3 can be cross-linked in vivo, and the cross-linked species were acetylated, implying that the interactions revealed by the Smc3/kleisin structure actually exist in complexes engaged in holding sister DNAs together.

Because of the presence of prolines (*10*), it is unlikely that α3 from bacterial kleisins extends as far up the coiled coil as is the case for Scc1. This difference between the cohesin and bacterial structures may therefore be genuine. To assess

[1]Department of Biochemistry, University of Oxford, Oxford, OX1 3QU, UK. [2]Max-Planck-Institut für Biochemie, 82152, Martinsried, Germany. [3]Medical Research Council (MRC) Genome Damage and Stability Centre, University of Sussex, Brighton BN1 9RQ, UK. [4]Dunn School of Pathology, University of Oxford, Oxford OX1 3RF, UK. [5]MRC Laboratory of Molecular Biology, Cambridge, CB2 0QH, UK.
*Corresponding author. E-mail: kim.nasmyth@bioch.ox.ac.uk (K.M.); jyl@mrc-lmb.cam.ac.uk (J.L.)

the N-terminal differences, we designed cysteine pairs, ScpAE39C-SmcH1043C and ScpAL42C-SmcQ1039C, which should be cross-linked if ScpA adopts the conformation observed in the ScpA/Smc crystal, and an alternative pair, E39C-Q1020C, which should be cross-linked only if they adopted the Smc3/Scc1 conformation. Our observation that, in *B. subtilis*, bis-maleimidoethane (BMOE) induces efficient cross-linking in vivo between the latter but not the former pairs suggests that ScpA binds to the Smc coiled coil by forming a four-helix bundle similar to that formed by Scc1 and Smc3 (fig. S4F).

Interaction between Scc1's NTD and Smc3's coiled coil is essential

The adverse effects of mutations within Scc1's NTD that affect its association with Smc3 (*11*) are explained by the structure. Three highly conserved leucine residues—L68, L75, and L89—line the surface of α3 that faces Smc3's coiled coil (Fig. 3A). In each case, substitution by lysine causes lethality, reduces association between Scc1 and Smc3 (*11*), and abrogates (in the cases of L75K and L89K) cohesin's association with centromeres (*12*). As expected, Scc1L89K abolished cross-linking between S1043C-C56 cysteine pairs (Fig. 3C). To address whether these defects arise from defective interaction with Smc3's coiled coil, we created a series of mutations intended to alter its surface without affecting coiled-coil formation per se (a comprehensive list of mutants and related phenotypes is provided in Fig. 3F). Lethality was caused by three mutations—L1019R, I1026R, and L1029R—that replaced hydrophobic side chains with charged ones on the surface of the coiled coil facing Scc1's α2 and α3 (Fig. 3B and fig. S5A). None of these mutations altered Smc3 levels or prevented Scc1's association with Smc1/Smc3 heterodimers in vivo (fig. S5B), presumably because association between Scc1's CTD and Smc1's ATPase head recruits the kleisin to heterodimers even when interaction between its NTD and Smc3 is compromised (*11*). Smc3L1029R also disrupted interaction with Scc1-N when coexpressed in *E. coli* (fig. S5F). In yeast cells, the same mutation reduced ultraviolet-induced cross-linking between Smc3A181bpa and Scc1 (fig. S5D) as well as cross-linking between Scc1Q76C and Smc3A181C (fig. S5C). Disruption of the hydrophobic nature of Smc3's coiled coil by Smc3L1019R, I1026R, and L1029R abrogated cohesin's ability to associate with centromeric DNAs in vivo and prevented acetylation of Smc3 by Eco1 (Fig. 3D and fig. S5E).

Introduction of charged residues into a hydrophobic interface precludes evaluation of the role of individual residues. For a more nuanced analysis, we focused on Y82, a conspicuous feature of α-, β-, and γ-kleisins (fig. S4D). Tetrad analysis revealed that Scc1Y82A caused slow growth at 30°C and lethality at 32°C (Fig. 3E and fig. S6A). Scc1Y82I had no obvious effect on proliferation but was synthetic lethal with a temperature-sensitive allele of *ECO1* (Eco1G211D). We conclude that insertion at this position in Smc3's coiled coil of a large aromatic residue has an important role in stabilizing its association with Scc1's NTD.

Although crucial, these hydrophobic interactions are insufficient. For example, lethality is also caused by substitution with glutamic acid of the highly conserved Smc3R1015 (Fig. 3B and fig. S6B)), which interacts with the equally conserved D92 within Scc1's α3. Contrary to previous observations, which were made on a version of Scc1 that was doubly tagged and contained a TEV protease cleavage site, D92K is in fact not lethal per se, although it does cause slow growth at 30°C and lethality at 37°C when Smc3 is tagged at its C terminus by PK3 (fig. S6C). Last, the finding that lethality is also caused by Scc1A47K (*11*), which alters a highly conserved alanine within Scc1's α2, confirms the importance of α2 (fig. S4A).

The KKD strand within the Smc3 ATPase head

The Smc3 ATPase heads have an irregular β strand at the top of their N-terminal lobe that contains an invariant aspartic acid residue (D114) next to a

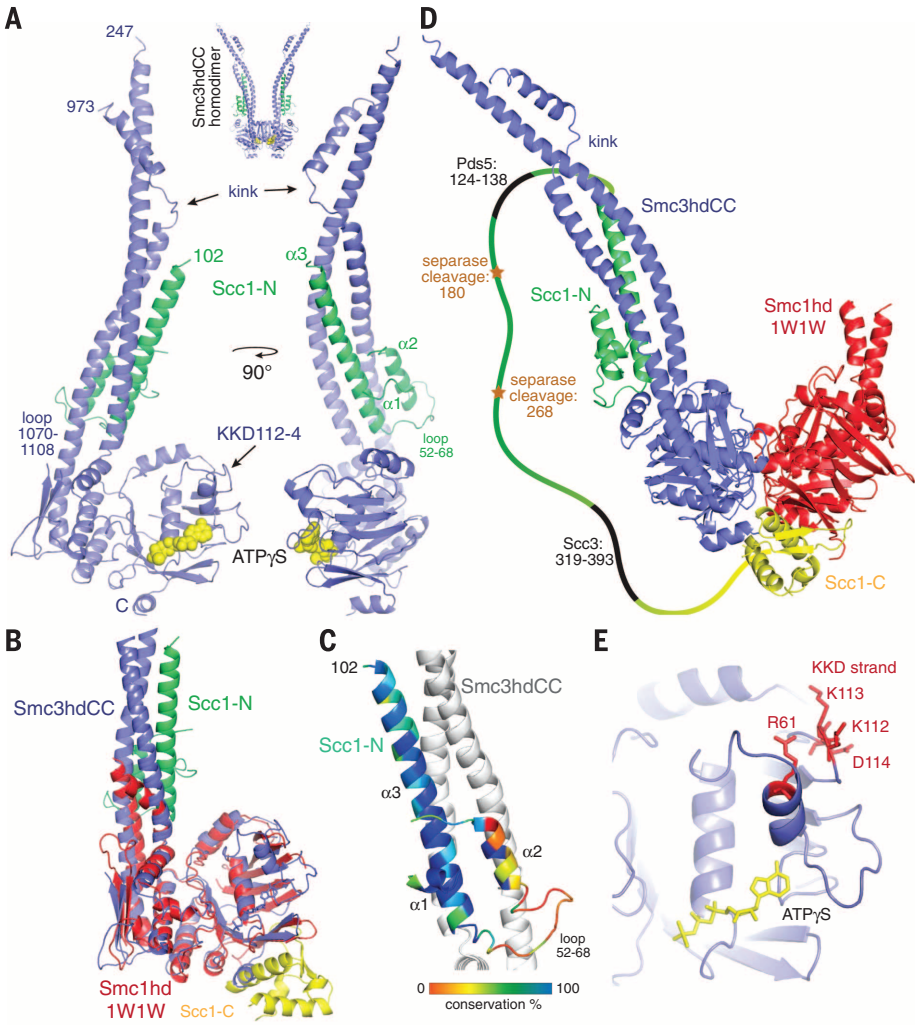

Fig. 1. Crystal structure of the Smc3hdCC:Scc1-N complex. (**A**) The coiled-coil segment of Smc3 (blue) is interrupted by a "kink." The NTD of Scc1, Scc1-N (green), binds to the coiled-coil segment of Smc3, leading to a four-stranded helical arrangement. (Inset) Aberrant homodimer formation of Smc3 head domains in the crystals. (**B**) A superposition of the Smc3hdCC:Scc1-N crystal structure (blue and green, respectively; this work) with Smc1hdCC:Scc1-C (red and yellow, respectively; PDB 1W1W) reveals that in addition to the ATPase fold, the position of the coiled-coil segments is conserved. Crucially, Scc1 binding is completely different for Smc3 and Smc1. (**C**) Sequence conservation of Scc1's NTD. (**D**) ATP binding leads to sandwich dimer formation of the head domains of Smc1 and Smc3, closing the ring temporarily. According to the ring model, Scc1 more permanently bridges the two head domains, which can be released through separase-mediated cleavage of Scc1 or in a separase-independent pathway through opening of the Smc3:Scc1 gate. Scc1 contains many more residues in the middle domain. Separase cleavage sites, Pds5 (*7*) and Scc3 binding sites are highlighted (*28*). (**E**) Detail of the KKD strand, whose acetylation by Eco1 reduces separase-independent cohesin release. It is far away from the nucleotide binding site on the head domain, but the acetylation state may influence the nucleotide binding site through the helix containing R61.

pair of highly conserved lysine residues (K112 and K113) whose acetylation by Eco1 is essential for sister chromatid cohesion (*13*, *14*). Our structure also reveals an adjacent α helix (R58-L64) whose base abuts the nucleotide and potentially links the latter to the KKD strand (Fig. 1E). The KKD strand, as well as other highly conserved Smc3-specific residues (S75, R107, and G110) in its vicinity (*15*), has a role in releasing cohesin from chromatin in a process dependent on cohesin's Wapl, Pds5, and Scc3 regulatory subunits. Acetylation of K112 and K113 by Eco1 neutralizes this activity and stabilizes cohesin's association with chromatin. Given that release is thought to involve transient dissociation of Scc1's NTD from Smc3, creating a gate through which DNA exits the ring, it is striking that the KKD strand is situated some distance (minimal 25 Å) from the part of Smc3 that binds Scc1, its coiled coil.

To address the function of the R58-L64 helix, we investigated the role of two highly conserved Smc3-specific residues (fig. S4C), Smc3R61 and E59. Replacement of R61 by glutamic acid or glutamine was lethal, whereas replacement by isoleucine or alanine was not (fig. S6D). In contrast, replacement of E59 by either alanine or arginine had little or no effect on cell proliferation. To address whether cohesin containing Smc3R61Q loads onto chromosomes, we compared the distribution of green fluorescent protein (GFP)–tagged Smc3R61Q and wild-type Smc3 in living cells carrying an untagged endogenous Smc3 gene. Smc3R61Q-GFP failed to accumulate at kinetochores or to form pericentromeric barrels during G2/M, implying that the mutant protein cannot load onto chromosomes, at least in the vicinity of centromeres (Fig. 3D). R61 is close to K112 and K113 (Fig. 1E), whose acetylation by Eco1 not only blocks release but also very possibly blocks cohesin's ability to engage in a loading reaction capable of producing cohesion (*16*). It is conceivable, therefore, that R61 has some role in relaying the state of modification of the KKD strand to Smc3's nucleotide binding pocket. Because the Smc3K112Q K113Q double mutation is also lethal and reduces cohesin's loading onto chromosomes (*13*, *17*), it is possible that in their unmodified form, K112 and K113 have a role in promoting cohesin loading and that they do so by influencing Smc3's ATPase activity in a manner involving R61. Thus, the KKD strand might be concerned with Scc2/4–mediated loading of cohesin onto chromosomes as well as Wapl-mediated release.

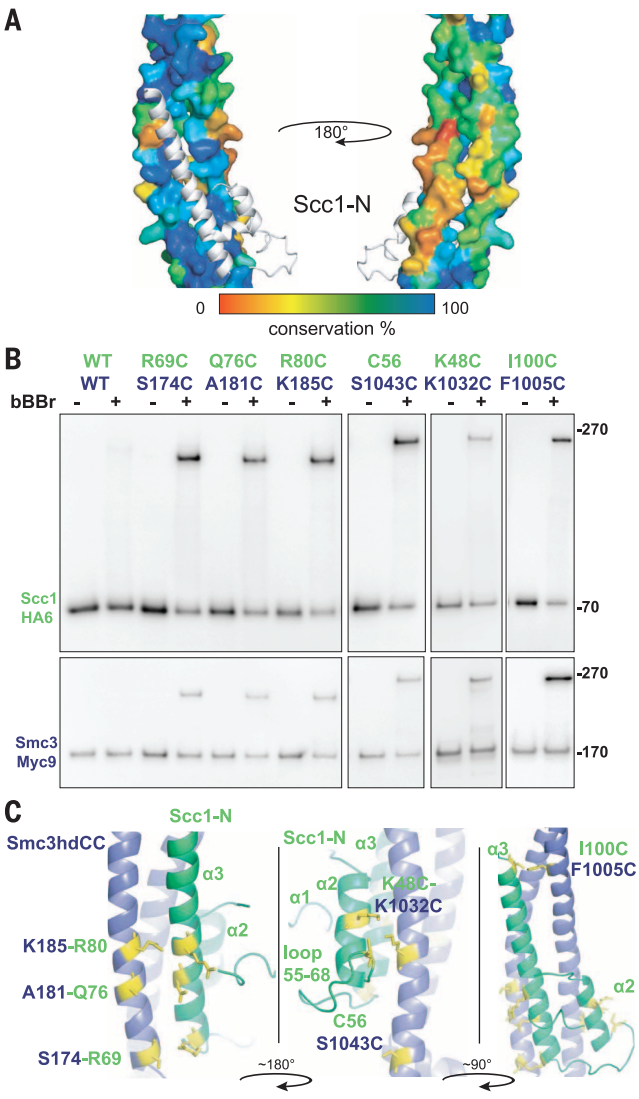

Fig. 2. Testing the Smc3-kleisin crystal structure. (**A**) Conservation of Smc3's coiled coil. The surface associated with Scc1 is highly conserved, but the solvent-exposed side is not. (**B**) Thiol-specific cross-linking (bBBr) between α2 and α3 of Scc1-N and Smc3's coiled coil (CC) after immunoprecipitation of Scc1-HA6. Cross-linking specific to K48C-K1032C was observed in cells expressing C56S (K19796, K19769, K19727, K19732, K19764, K23102, and K23103). All mutations were functional, and all observed cross-links were dependent on a pair of cysteine substitutions. (**C**) Scc1-N α2 and α3 helices (green), Smc3 coiled coil (Smc3CC, blue), and substituted residues (yellow).

Cohesin trimers hold sister DNAs together in live cells

To address whether simultaneous interaction of the three Smc/kleisin interfaces actually creates rings in vivo, living cells expressing Smc1-myc9, Scc1-PK6, and Smc3-Halo were incubated with BMOE to cross-link one, two, or three interfaces. Scc1-PK6 was then immunoprecipitated. In the presence of the tetramethylrhodamine (TMR) ligand, Smc3-Halo becomes labeled and fluorescent and was visualized after SDS–polyacrylamide gel electrophoresis by scanning gels at 545 nm (Fig. 4B). Smc1-myc9 and Scc1-PK6 were detected by means of Western blotting (fig. S7A). Dimeric molecules were created if cysteine pairs were present at single interfaces, and trimers were created when cysteine pairs were present at two interfaces (Fig. 4B). Cross-linking cohesin containing cysteines at all three interfaces generated a new form form (Ci) whose electrophoretic mobility was slower than that of all three trimeric forms created by cross-linking at merely two out of the three interfaces. This form presumably arises from the creation of circular molecules owing to the simultaneous cross-linking of all three interfaces of tripartite rings. The fraction of linear and circular trimers was roughly consistent with cross-linking at each of the three interfaces occurring independently (fig. S7C). Similar results were obtained by cross-linking with bBBr after immunoprecipitation (fig. S7B). Thus, most cohesin inside living yeast cells has the form of a heterotrimeric ring. Western blotting by using antibodies specific for acetylated Smc3 (*17*) showed that the Ci form was acetylated to a degree similar to that of molecules that had not been chemically circularized (Fig. 4B, last lane). Acetylation was detected in cross-linked species created in vivo by several different cysteine pairs (Fig. 4A). Because cohesion is mediated only by acetylated complexes (*13*, *14*), these data suggest that the cohesin complexes responsible for holding sister DNAs together are also circular Smc1/Smc3/Scc1 heterotrimers.

It has been suggested that Scc1 links the ATPase heads of different Smc1/Smc3 heterodimers, creating dimeric rings or multimeric chains (*18*). According to this scenario, the Ci form could conceivably be a tetramer containing Smc subunits from two Smc1/3 heterodimers. To address whether Ci contains more than one Smc3 molecule, we compared the amount of Halo-tagged Ci associated with PK- and hemagglutinin (HA)–tagged proteins from Scc1-PK6/Scc1-PK6, Smc3-HA6/Smc3-Halo diploids after in vivo cross-linking. This showed that little or no Smc3-Halo is present in Ci molecules that had

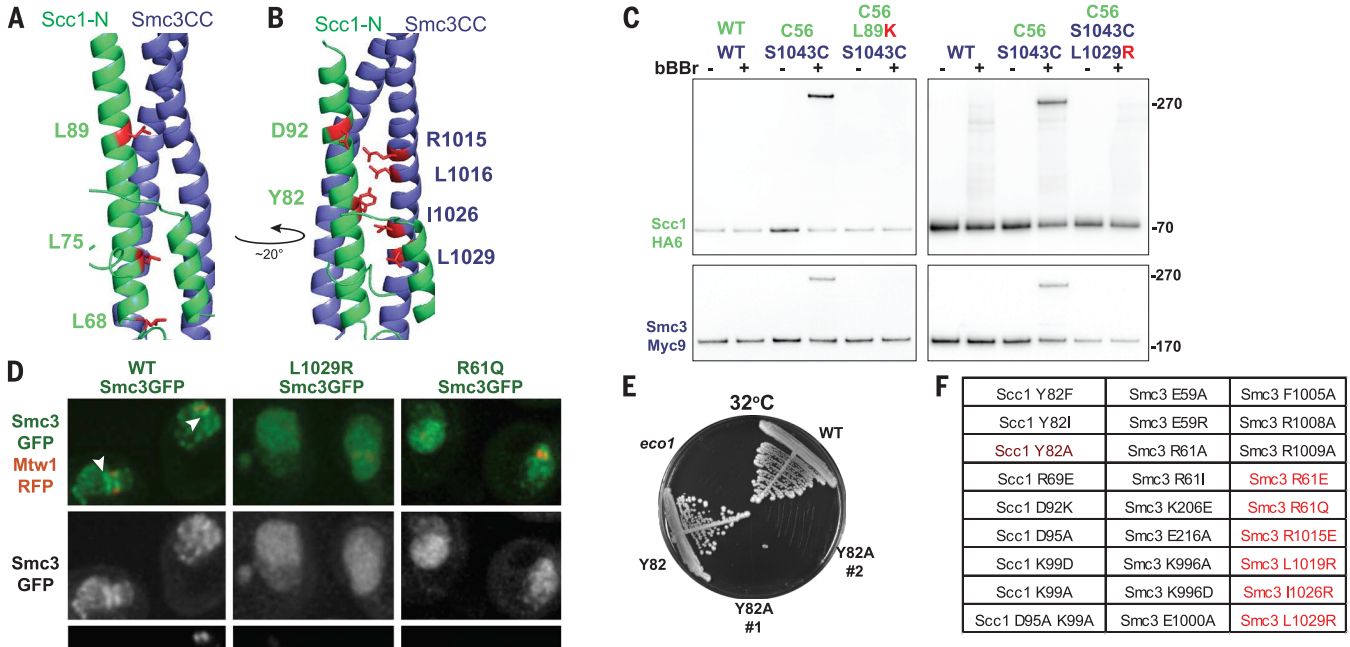

Fig. 3. Functional analysis of the Smc3-kleisin structure. (**A**) Essential Scc1-N residues (*11*) situated within the Smc3-kleisin interface. (**B**) Conserved residues in Scc1-N (D92 and Y82) and Smc3CC (R1015, L1019, I1026, and L1029), whose mutation disrupts interaction and causes lethality. (**C**) Abolition of Scc1-N/Smc3CC cross-linking by Scc1L89K (K19796, K23144, and K23145) and Smc3L1029R (K23146, K23128, and K23129) as measured by cross-linking C56-S1043C with bBBr after immunoprecipitation of Scc1-HA6. Western blots of Smc3-myc9 and Scc1-HA6 are shown. (**D**) Diploid cells expressing ectopic WT or mutant Smc3-GFP, with white arrowheads pointing at the cohesin pericentromeric barrel structure absent in the case of L1029R and R61Q (K23107-23109). (**E**) Scc1Y82A is lethal at 32°C (K699, K16296, and K23105-6). (**F**) A summary of mutations created and characterized. Lethal (red) and temperature-sensitive (brown) mutations, both in Scc1 and Smc3, were found. Shown is the viability of Scc1D95A, K99D, K99A, and D95A K99A mutants (K23111-23117).

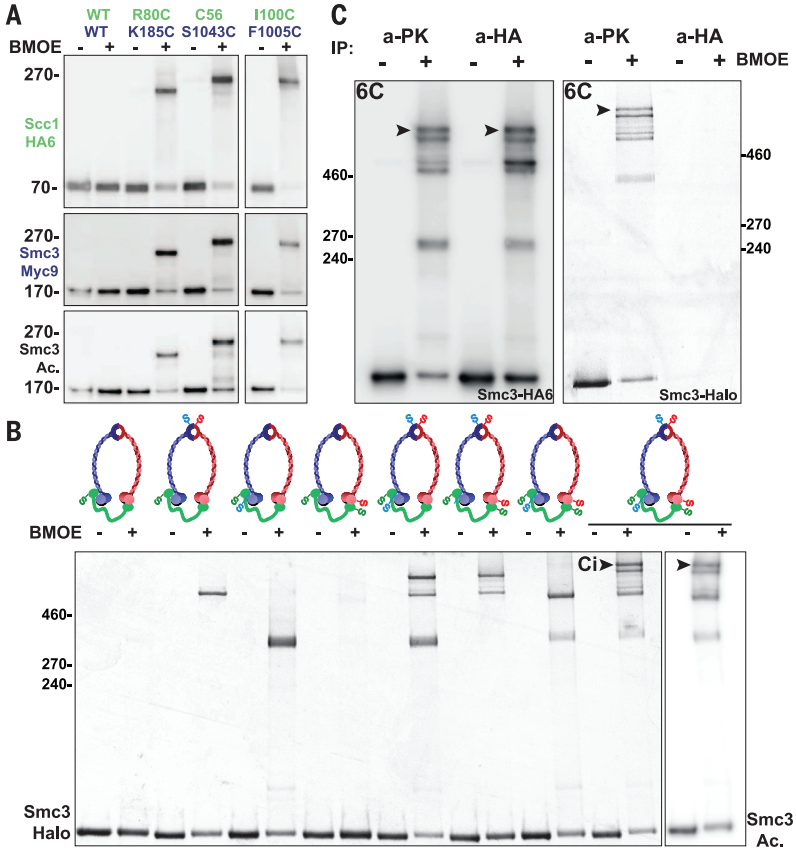

Fig. 4. Cohesin forms heterotrimeric rings in vivo. (**A**) In vivo thiol-specific cross-linking (BMOE) between α2 and α3 of Scc1-N and the Smc3 coiled coil (CC) followed by immunoprecipitation of Scc1-HA6. In all shifted bands, Smc3 is acetylated (K19796, K19732, K19764, and K23103). (**B**) In vivo thiol-specific cross-linking of the three Smc1/Smc3/Scc1 interfaces followed by immunoprecipitation of Scc1-PK6 and observation of TMR fluorescence associated with Smc3-Halo. A circular form (Ci) only appears when all three interfaces are linked (black arrowheads). Western blotting by use of an antibody specific for acetylated K113 shows that Ci is acetylated (last lane) (strains K22013-K22020). (**C**) Cohesin forms heterotrimeric rings but not higher-order complexes. Halo-tagged Ci (black arrowhead) is associated with PK- and HA-tagged proteins from Scc1-PK6/Scc1-PK6, Smc3-HA6/Smc3-Halo diploids after in vivo cross-linking. No Smc3-Halo is present in form Ci molecules that had been immunoprecipitated with HA antibodies, implying that they are circular trimers, not tetramers (K22590).

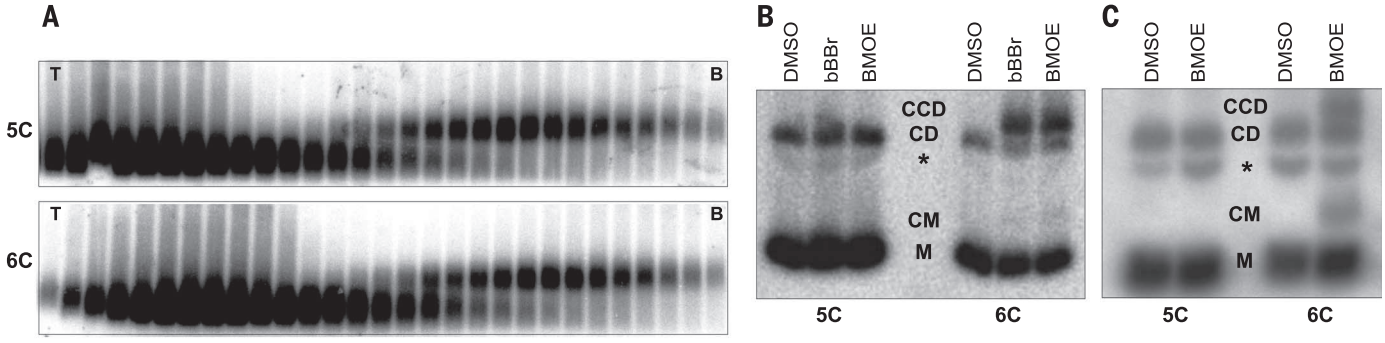

Fig. 5. Heterotrimeric cohesin rings trap sister DNAs both in vitro and in vivo. (**A**) Dimers of a 2.3-kb circular minichromosome were isolated by using sucrose gradients (T, top; B, bottom) from strains containing five (5C) or six (6C) cysteines within the Smc1/Smc3/Scc1 interfaces (K20300 and K20279). (**B**) Electrophoresis of dimers denatured with SDS after isolation from sucrose gradients and cross-linking with bBBr or BMOE. DNAs detected by means of Southern blotting. (**C**) Electrophoresis of Scc1-PK6 immunoprecipitated DNAs denatured with SDS after in vivo BMOE cross-linking of cycling cells. DNAs detected by means of Southern blotting. M, monomeric circles: CM, catenated monomers; asterisk, nicked DNA; CD, catenated dimers; and CCD, cohesin catenated dimers (K20280 and K20279).

been immunoprecipitated with HA antibodies, implying that they are circular heterotrimers and not tetramers or multimers (Fig. 4C). We used a similar method, albeit without cross-linking, to show that acetylated wild-type Smc3 cannot be co-immunoprecipitated by a myc-tagged version when extracts were prepared from Smc3/Smc3-myc18 diploids (fig. S7E).

Sister DNAs are entrapped by cohesin trimers

To test whether cross-linking all three interfaces of the cohesin ring entraps sister DNAs in a covalent topological embrace, we isolated dimers of a 2.3-kb circular minichromosome (Fig. 5A), treated them with bBBr or BMOE, and subjected them to gel electrophoresis after denaturation (*19*). In the absence of cross-linker, most minichromosome DNAs detected with Southern blotting migrated as closed circular monomers (Fig. 5B, M), whereas 10 to 20% migrated as monomeric nicked circles or catenated supercoils (CD). With cysteine pairs at all three interfaces, both cross-linkers caused the appearance of dimers (CCD) that migrate more slowly than catenated supercoils (Fig. 5B) (*9*). No such dimers were formed when minichromosomes were isolated from a strain lacking a single one of the six "interface" cysteines (Fig. 5B). We estimated that the fraction of monomeric DNAs converted to dimers by cross-linking was ~25%, which is similar to the efficiency of cohesin's chemical circularization in vivo (Fig. 4B) and in vitro (fig. S7B). Crucially, sister (CCD) as well as monomeric (CM) DNAs were catenated in this manner by chemically circularized cohesin when living yeast cells were treated with BMOE (Fig. 5C), indicating that cohesin rings entrap sister DNAs in vivo.

Discussion

Our crystal structure of an Smc3/Scc1 complex provides a mechanism by which a single Scc1 polypeptide links the ATPase heads of Smc1/Smc3 heterodimers, creating a heterotrimeric ring structure. Using thiol-specific chemical cross-linking, we demonstrate that cohesin complexes holding sister chromatids together in vivo do indeed have the configuration of heterotrimeric rings and that sister minichromosome DNAs are entrapped within these in vivo. The interactions between Smc1/3 hinges, Smc1 ATPase/Scc1-C, and Smc3CC/Scc1-N are all very stable (*4*, *20*, *21*). Intact cohesin rings are therefore likely to be extremely durable in the absence of specific mechanisms to disrupt them. Such a feature is desirable for a complex that must hold sister DNAs together for extended periods of time, which may last for several decades in the case of human oocytes.

Two mechanisms are known to remove cohesin from chromosomes. Best understood is cleavage of the central domain of Scc1 (*22*) and its meiotic counterpart Rec8 (*23*) by separase, an event that triggers sister chromatid disjunction at the onset of anaphase. The simplest explanation for this phenomenon is that the three interactions that create tripartite cohesin rings are both necessary and sufficient to entrap sister DNAs, and separase merely destroys topological entrapment. The second mechanism is separase-independent, occurs throughout the cell cycle, and is especially active during prophase, when most cohesin is removed from chromosome arms (*24*, *25*). The releasing activity responsible for this phenomenon is associated with cohesin itself; involves its Wapl (*26*, *27*), Pds5, and Scc3 subunits (*15*); and is blocked by fusion of Smc3 to Scc1. Our finding that Smc3 R61 possibly links the KKD strand to the Smc3's adenosine 5´-triphosphate (ATP) binding pocket raises the possibility that acetylation, which blocks releasing activity, may directly regulate ATPase activity and vice versa.

Sequence comparisons suggest that most if not all eukaryotic Smc/kleisin complexes have a configuration similar to that of cohesin's ring. Because all three interfaces of cohesin's ring and those of bacterial Smc/kleisin complexes are structurally homologous, this class of complex must have been present in the last common ancestor of all living organisms and may be an indispensable feature of DNA genomes.

REFERENCES AND NOTES

1. J. M. Peters, A. Tedeschi, J. Schmitz, *Genes Dev.* **22**, 3089–3114 (2008).
2. K. Nasmyth, *Nat. Cell Biol.* **13**, 1170–1177 (2011).
3. S. Gruber, C. H. Haering, K. Nasmyth, *Cell* **112**, 765–777 (2003).
4. C. H. Haering, J. Löwe, A. Hochwagen, K. Nasmyth, *Mol. Cell* **9**, 773–788 (2002).
5. S. Gruber *et al.*, *Cell* **127**, 523–537 (2006).
6. K. L. Chan *et al.*, *Cell* **150**, 961–974 (2012).
7. K. L. Chan *et al.*, *Proc. Natl. Acad. Sci. U.S.A.* **110**, 13020–13025 (2013).
8. F. Bürmann *et al.*, *Nat. Struct. Mol. Biol.* **20**, 371–379 (2013).
9. C. H. Haering *et al.*, *Nature* **454**, 297–301 (2008).
10. A. Schleiffer *et al.*, *Mol. Cell* **11**, 571–575 (2003).
11. P. Arumugam *et al.*, *Curr. Biol.* **16**, 1998–2008 (2006).
12. B. Hu *et al.*, *Curr. Biol.* **21**, 12–24 (2011).
13. E. Unal *et al.*, *Science* **321**, 566–569 (2008).
14. T. Rolef Ben-Shahar *et al.*, *Science* **321**, 563–566 (2008).
15. B. D. Rowland *et al.*, *Mol. Cell* **33**, 763–774 (2009).
16. F. Beckouët *et al.*, *Mol. Cell* **39**, 689–699 (2010).
17. T. Sutani *et al.*, *Curr. Biol.* **19**, 492–497 (2009).
18. C. E. Huang, M. Milutinovich, D. Koshland, *Philos. Trans. R. Soc. London B Biol. Sci.* **360**, 537–542 (2005).
19. D. Ivanov, K. Nasmyth, *Mol. Cell* **27**, 300–310 (2007).
20. C. H. Haering *et al.*, *Mol. Cell* **15**, 951–964 (2004).
21. A. Kurze *et al.*, *EMBO J.* **30**, 364–378 (2011).
22. F. Uhlmann *et al.*, *Nature* **400**, 37–42 (1999).
23. S. B. Buonomo *et al.*, *Cell* **103**, 387–398 (2000).
24. A. Losada *et al.*, *Genes Dev.* **12**, 1986–1997 (1998).
25. I. Sumara *et al.*, *J. Cell Biol.* **151**, 749–762 (2000).
26. R. Gandhi *et al.*, *Curr. Biol.* **16**, 2406–2417 (2006).
27. S. Kueng *et al.*, *Cell* **127**, 955–967 (2006).
28. M. B. Roig *et al.*, *FEBS Lett.* **16**, 3692–3702 (2014).

ACKNOWLEDGMENTS

T.G.G. is supported by a European Molecular Biology Organization long-term fellowship (ALTF 2008-127) and the John Fell Fund (132/108). The work was funded by the Medical Research Council (U10518432 to J.L., C573/A11625 to J.C.S.), the Wellcome Trust (095514/Z/11/Z to J.L., 091859/Z/10/Z to K.N.), Cancer Research UK (C573/A 12386 to K.N.), and the MitoSys project (FP7/2007-2013 under grant agreement 241548 to K.N.).

SUPPLEMENTARY MATERIALS

www.sciencemag.org/content/346/6212/963/suppl/DC1
Materials and Methods
Figs. S1 to S7
Tables S1 to S2
References (*29*–*36*)

3 June 2014; accepted 26 September 2014
10.1126/science.1256917

Closing the cohesin ring: Structure and function of its Smc3-kleisin interface

Thomas G. Gligoris *et al.*

Science **346**, 963 (2014);
DOI: 10.1126/science.1256917

www.sciencemag.org/content/346/6212/963/suppl/DC1

Supplementary Material for

Closing the cohesin ring: Structure and function of its Smc3-kleisin interface

Thomas G. Gligoris, Johanna C. Scheinost, Frank Bürmann, Naomi Petela, Kok-Lung Chan, Pelin Uluocak, Frédéric Beckouët, Stephan Gruber, Kim Nasmyth* Jan Löwe*

*Corresponding author. E-mail: kim.nasmyth@bioch.ox.ac.uk (K.M.); jyl@mrc-lmb.cam.ac.uk (J.L.)

Published 21 November 2014, *Science* **346**, 963 (2014)
DOI: 10.1126/science.1256917

This PDF file includes:

Materials and Methods

In vivo photo cross-linking

Site-directed mutagenesis was used to replace each one of the first 142 codon triplets of *S. cerevisiae* Scc1 by an amber codon (TAG) in an episomal vector (YEpLac181-Scc1-HA3). Of the designed replacements ca. 80% were obtained. Substitutions were introduced into yeast cells in combination with an episomal plasmid bearing an amber-codon-recognizing tRNA and a modified tRNA synthetase(*29*) able to load the amber tRNA with the unnatural photoreactive amino-acid *p*-benzoylphenylalanine (bpa, Bachem). Similarly, using YepLac181-Smc3-myc9 and YepLac181-Smc3-HA6 were employed when making substitutions within the Smc3 ATPase head and coiled coil. Wild type versions of Scc1 and/or Smc3 were counter selected on 5-FOA plates (supplemented with 1-3 mM bpa), and strains assessed for viability and dependence to grow on bpa. For UV-induced cross-linking experiments, cells were grown to log phase in rich medium supplemented with 1 mM bpa and approximately 10 OD_{600nm} units re-suspended in 1 ml ice cold PBS and irradiated with UV light (365nm) for 3x5 min in a Spectrolinker device (Spectroline, total energy of ca. $5.3x10^6$ μJ/cm^2). Total protein extraction followed using the standard glass bead TCA method. 25 μg of total protein per sample were analyzed by SDS-PAGE and Western blotting.

Cyanogen bromide chemical cleavage

Photo cross-linking was performed as described above. Strains were grown in YEPD at 30 °C to OD_{600nm} = 1 in cultures supplemented with 1 mM bpa. Cells were broken in 500 μl EBX lysis buffer (50 mM HEPES pH8.0, 100 mM KCl, 2.5 mM $MgCl_2$, 0.05% NP40, 0.25% Triton-X) containing 1 mM DTT, DNase I (1:1,000), Roche Complete Protease Inhibitors (2X) and PMSF (1 mM), lysed in a FastPrep-24 (MP Biomedicals) for 2x1 min at 6 m/s with 500 μl of acid-washed glass beads (425-600 μm, Sigma) and lysates cleared (15 min, 15 k*g*). Immuno-precipitations against myc9-Scc1 were performed using anti-myc antibody (9E10) and protein G sepharose (Amersham Biosciences) at 4 ^oC for 1.5 hrs. Immuno-precipitated complexes on beads (30 μl) were treated with 1-2 crystals of CNBr in 70 μl of formic acid. Samples were left incubating overnight at room temperature. After cleavage, water was added to a final volume of 1000 μl, BSA was added to a final concentration of 0.1 mg/ml to improve yield of recovered protein after TCA precipitation (TCA final concentration 10%). Protein was pelleted and washed with ice cold 50 mM Tris/HCl in 80% acetone. Pellets were suspended in SDS loading buffer and loaded onto 15% Tris-glycine gels before Western blotting.

In vivo chemical cross-linking

Strains were grown in YEPD at 30 °C to OD_{600nm} = 0.8 and arrested in nocodazole for 1.5 h. 60 OD units were washed in ice-cold PBS, then re-suspended in 1 ml ice-cold PBS. The suspensions were then split into 2 x 600 μl and 25 μl BMOE (stock: 125 mM in DMSO, 5 mM final) or DMSO was added for 6 min on ice. Cells were washed with 2 x 2 ml ice-cold PBS containing 5 mM DTT, resuspended in 500 μl EBX lysis buffer

containing 1 mM DTT, benzonase (1:1000), RNase (0.1 mg/ml), Roche Complete Protease Inhibitors (2X) and PMSF (1 mM), lysed in a FastPrep-24 (MP Biomedicals) for 3 min at 6 m/s with 500 µl of acid-washed glass beads (425-600 µm, Sigma) and lysates cleared (5 min, 12 k*g*). Protein concentrations were adjusted after Bradford assay and cohesin immuno-precipitated using anti-PK antibody (AbD Serotec, 1 h, 4 °C) and protein G dynabeads (1 h, 4 °C with rotation) in the presence of Halo-TMR substrate (5 µM). Beads were washed with 2 x 1 ml lysis buffer, resuspended in 50 µl 2x sample buffer, incubated at 95°C for 5 min and 40 µl supernatant loaded onto a 5% SDS-PAGE gel. TMR fluorescence was detected on a Fuji FLA-7000 instrument using Cy3 presets. For Western blotting, 5 µl were separated on 3-8% Tris-acetate gels, blotted by semi-dry transfer, probed with anti-myc (Santa Cruz) or anti-PK (AbD Serotec) antibodies and visualized on a LI-COR Odyssey Fc. For Southern blotting, pull-downs of lysates (in 25 mM Hepes pH 8.0, 50 mM KCl, 50 mM $MgSO_4$, 10 mM trisodium citrate, 25 mM sodium sulfite, 0.25% triton-X, Roche Protease Inhibitor, 1 mM PMSF, 2 mM DTT, 0.1 mg/ml RNase) containing a circular 2.3 kb mini-chromosome were performed as above, DNA was eluted in 30 µl 1% SDS with DNA loading dye (65 °C, 4 min) and run on 0.8% agarose gels containing ethidium bromide (1.4 V/cm, 22h, 4 °C).

In vitro chemical cross-linking

Yeast cells from 100 ml YEPD cultures were harvested by centrifugation at OD_{600} = 0.6. Cells were resuspended in 500 µl EBX lysis buffer with 1 mM DTT, 0.5 mM PMSF in isopropanol, 0.1% DNaseI, 1 complete EDTA-free protease inhibitor cocktail tablet (Roche Diagnostics) per 50 ml solution). 500 µl of acid-washed glass beads (425-600 µm, Sigma) were added to the suspension and the cells lysed in a FastPrep-24 instrument (MP Biomedicals) for 2 min at 4.5 m/s. Lysates were spun down for 5 min at 4 °C, 15,000 x*g*, the supernatant removed from the beads and incubated with 100 µl anti-HA sepharose beads (GE Healthcare) for 1.5 h at 4 °C or with 100 µl 9E10 anti-myc serum for 1h at 4 °C and 100 µl of protein G sepharose beads (GE Healthcare) for a further 30 min at 4 °C. The beads were isolated by gentle centrifugation, washed once in lysis buffer (without DTT) before cross-linking. bBBr was added to a final concentration of 0.13 mM and the samples were incubated at 4°C for 10 min. The supernatant was removed, the pellet resuspended in 100 µl 2× SDS loading buffer and the suspension was denaturated at 95 °C for 10 min. Samples were spun down for 5 min at 15,000 x*g* and 5 or 15 µl of the supernatant ran on a 3-8% Tris-acetate gel at 45 mA/gel for 70 min, followed by Western blotting and immuno-detection of the HA or myc epitopes.

Co-expression of Smc3hdCC and Scc1 in *E. coli* and purification of the Smc3-Scc1 complex

A pET28a based plasmid with a version of Smc3NBD and a large part of the emerging coiled coil (Smc3hdCC = MAY_2-S_{260}linkerD_{971}-V_{1230}StrpII) was co-expressed in BL21(DE3)RIPL *E. coli* with a pET21d-based plasmid of Scc1 (Scc1-N = M_1-N_{115}-6xHIS). Cells were grown at 37°C to OD_{600nm} = 1, temperature was shifted and when reached 16 °C expression was induced by adding IPTG to a final concentration of 1 mM. Cell pellets were resuspended in TEN_{150} buffer (50 mM Tris pH 7.5, 2 mM EDTA, 150 mM NaCl supplemented with 1 EDTA-free Roche protease inhibitor cocktail tablet per

50 ml) and suspensions passed through a French press at 20 kpsi at 4°C, supplemented with 1 mM PMSF, sonicated on ice, and spun for 1.5 hrs at ~25,000 *g*. The clarified extract was first passed through a Strep-Tactin column (IBA) , the column washed (TN_{200}), protein was eluted with desthiobiotin and the eluate was passed through a TALON column (Clontech). After loading the column was washed (TN_{200} with 10 mM imidazole) and captured protein was eluted with 0.5 M imidazole, concentrated in Vivaspin columns (30 kDa cut-off, Vivaproducts) and loaded onto a 16/600 Superdex 200 gel filtration column (GE Healthcare) in 50 mM Tris pH 7.5, 150 mM NaCl, 1 mM βME. For the experiment in panel Fig. S4F, a modified version of Smc3hdCC with a Flag tag was used. After elution and gel filtration, protein was concentrated with Vivaspin columns and crosslinking was performed using bBBr at a final concentration of 0.25 mM for 15 mins on ice.

Yeast live-cell imaging

All strains used for live-cell imaging are diploid. Exponentially growing cells in YEP medium plus 10% glucose were placed on 2.5% agarose pads. Live cell imaging was performed under a spinning disk confocal system (PerkinElmer UltraVIEW) with an EMCCD camera (Hamamatsu) mounted on an Olympus IX8 microscope with Olympus 100x 1.35 NA objectives. Image acquisition was done at room temperature. Seventeen Z-stack images with 0.2 μm intervals were acquired and deconvoluted with Volocity software. Fresh samples were prepared every 10 minutes.

Sucrose gradients and minichromosome separation in SDS-agarose gels

These experiments were performed as described previously (9, 30).

Crystallization, data collection and structure determination

Crystallization conditions were found using LMB's in-house nanolitre crystallization facility (*31*). Crystals were grown by vapor diffusion, equilibrating drops of 100 nl reservoir plus 100 nl protein solution (30 mg/ml in 50 mM Tris pH 7.5, 150 mM NaCl, 1 mM βME, 1 mM ATPγS, 2 mM $MgSO_4$) against reservoirs containing 100 mM imidazole/HCl pH 7.0 and 0.5-1 % (w/v) PEG 200 (vapor diffusion dilutes sample, salting-incrystallization). Crystals were cryo-protected by adding reservoir solution supplemented with 50-60 % (w/v) PEG 200, before flash freezing in liquid nitrogen. Datasets were collected at Diamond Light Source (Harwell, UK) beamlines I24, I02 and I03 on Pilatus detectors and indexed and integrated with XDS (*32*). Data reduction was performed with SCALA(*33*). Molecular replacement with various sequence-related Smc head domains and PHASER (*34*) produced weak hits that were verified to be correct because of ABC ATPase dimer formation. The resulting electron densities were unbuildable so additional phase information was obtained with a SAD experiment on SeMet substituted crystals that were grown under identical conditions. Most selenium sites were found by cross-phasing anomalous differences with the molecular replacement phases and all phase information was then used in order to obtain an electron density map at 3.3 Å resolution, which was of good to adequate quality. The model was manually built and adjusted using MAIN (*35*) and refined with REFMAC (*36*). However, the residue assignment on helices α1 and α2 of Scc1 remained uncertain because of poor

density for the loop between α2 and α3 and a lack of SeMet residues in that area. We therefore verified our model by introducing the mutation K52M into Scc1's α2 and repeated the SAD experiment, which after phasing of the anomalous differences showed a peak at the correct position. The structure and structure factors have been deposited in the Protein Data Bank (PDB) with accession code 4UX3 and statistics of the data and model are summarized in Table 1.

Supplementary Figures S1-S7

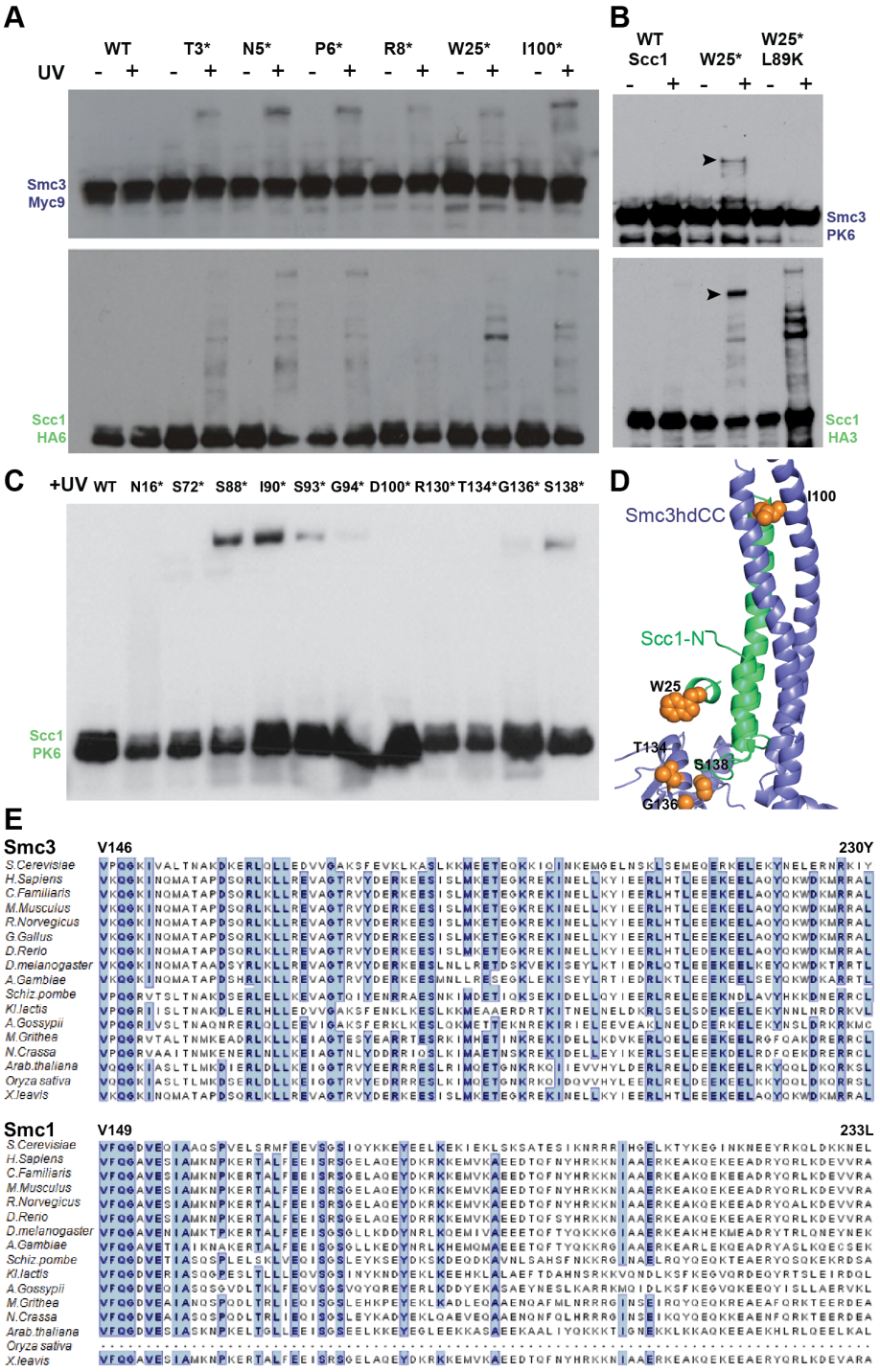

Figure S1. In vivo photo cross-linking shows that Scc1's NTD binds Smc3.
We investigated the Smc3/kleisin interaction by in vivo photo cross-linking (*7*), using an orthogonal tRNA and tRNA synthetase pair to incorporate the photoreactive amino acid *p*-benzoyl-phenylalanine (bpa) at nonsense codons at each one of Scc1's N-terminal 142 codons (*7*). Several substitutions by bpa facilitated cross-linking with Smc3 upon UV irradiation of live yeast cells

(A) Western blotting after TCA protein precipitation of yeast strains bearing bpa replacements in Scc1 (T3, N5, P6, W25 and I100 in Scc1). Scc1-PK6 band shifts corresponding to cross-linked species are UV-dependent and contain Smc3.

(B) Scc1W25bpa UV-induced cross-linking as measured by Western blotting following immuno-precipitation of Scc1-HA3 is abolished by Scc1L89K (*11*)

(C) UV-induced cross-links between Scc1 and bpa replacing S88, I90, S93, G136, and S138 within Smc3's ATPase head.

(D) Bpa substitutions (orange spheres) giving rise to moderate UV-dependent cross-linking, located on the Smc3-kleisin structure.

(E) CLUSTALW alignment of the Smc3 and Smc1 amino-terminal sequences from various species highlighting identical residues in blue.

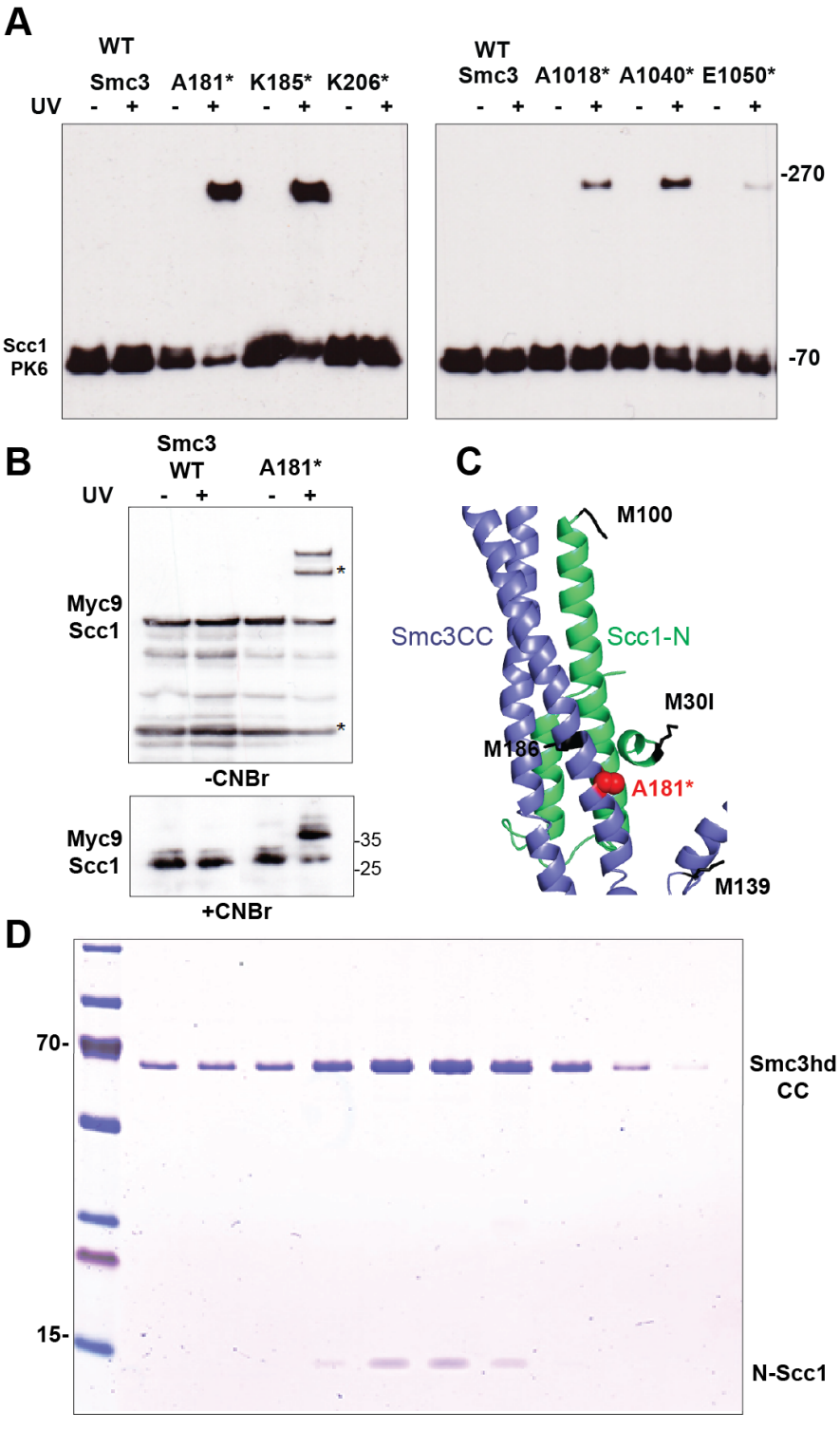
A
WT
Smc3
A181*
K185*
K206*
UV
WT
Smc3
A1018*
A1040*
E1050*
-270
-70
Scc1
PK6
B
Smc3
WT
A181*
UV
Myc9
Scc1
-CNBr
Myc9
Scc1
-35
-25
+CNBr
C
M100
Smc3CC
Scc1-N
M30I
M186
A181*
M139
D
70-
15-
Smc3hd
CC
N-Scc1

Figure S2. Scc1's NTD interacts with Smc3's coiled coil in vivo and in vitro.

(A) Immuno-precipitation of Smc3-HA6 after UV irradiation of live cells, followed by Western blotting against Scc1-PK6. Smc3 substitutions A181bpa, K185bpa, A1018bpa, A1040bpa, and E1050bpa but not K206bpa show low to high efficiency photo-crosslinking towards Scc1-PK6. Strains K20358-K20364.

(B) Immuno-precipitation of myc9-Scc1 after UV irradiation of live cells bearing Smc3 with A181bpa. Separase's cleavage fragment and the corresponding upshifted Smc3 cross-linked bands are indicated with an asterisk. Lower panel: cyanogen bromide (CNBr) induced cleavage after methionines creates a shift corresponding to the endogenous fragment flanking M139 and M186 in Smc3 (K20366, K20367).

(C) Ribbon diagram presenting the fragments generated by the CNBr methionine proximal cleavage described in panel (B). Scc1's endogenous M1 has been deleted, an N-terminal myc9 epitope was fused in frame and endogenous M30 was changed to I30. Endogenous Scc1M102, Smc3M139 and M186 generate a 30 kDa Scc1 and a 5 kDa Smc3 fragment. Smc3 cleavage with CNBr creates no other 5 kDa predicted fragment which could contain the cross-linking residue Smc3A181bpa.

(D) A complex containing the first 115 N-terminal residues of Scc1 and the Smc3 ATPase head along with a segment of its coiled coil was purified from a BL21(DE3)RIPL *E. coli* derived strain (TGBL203) and characterized by gel filtration. Proteins visualized by Coomassie staining following SDS-PAGE.

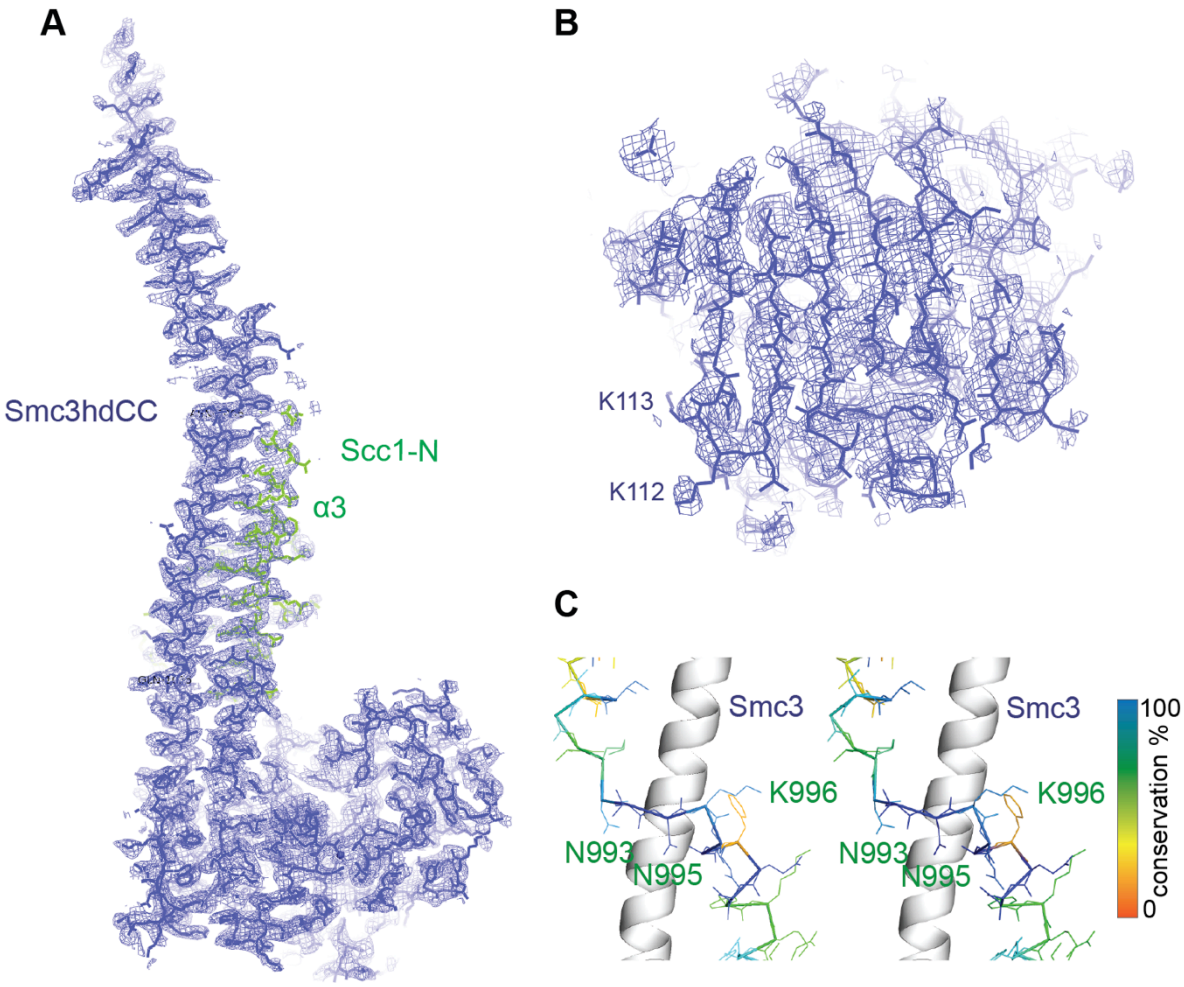

Figure S3. Details of the Smc3/kleisin structure.

(A) 2Fo-Fc electron density maps of the Smc3 (Smc3hdCC) and Scc1-N complex with Scc1-N helix α3 highlighted (green).

(B) 2Fo-Fc electron density map of the KKD strand area of the ATPase head. The electron density of the Smc ATPase's beta sheet has lower quality compared to the rest of the structure.

(C) Stereo view of the pronounced conserved kink of the Smc3 coiled coil.

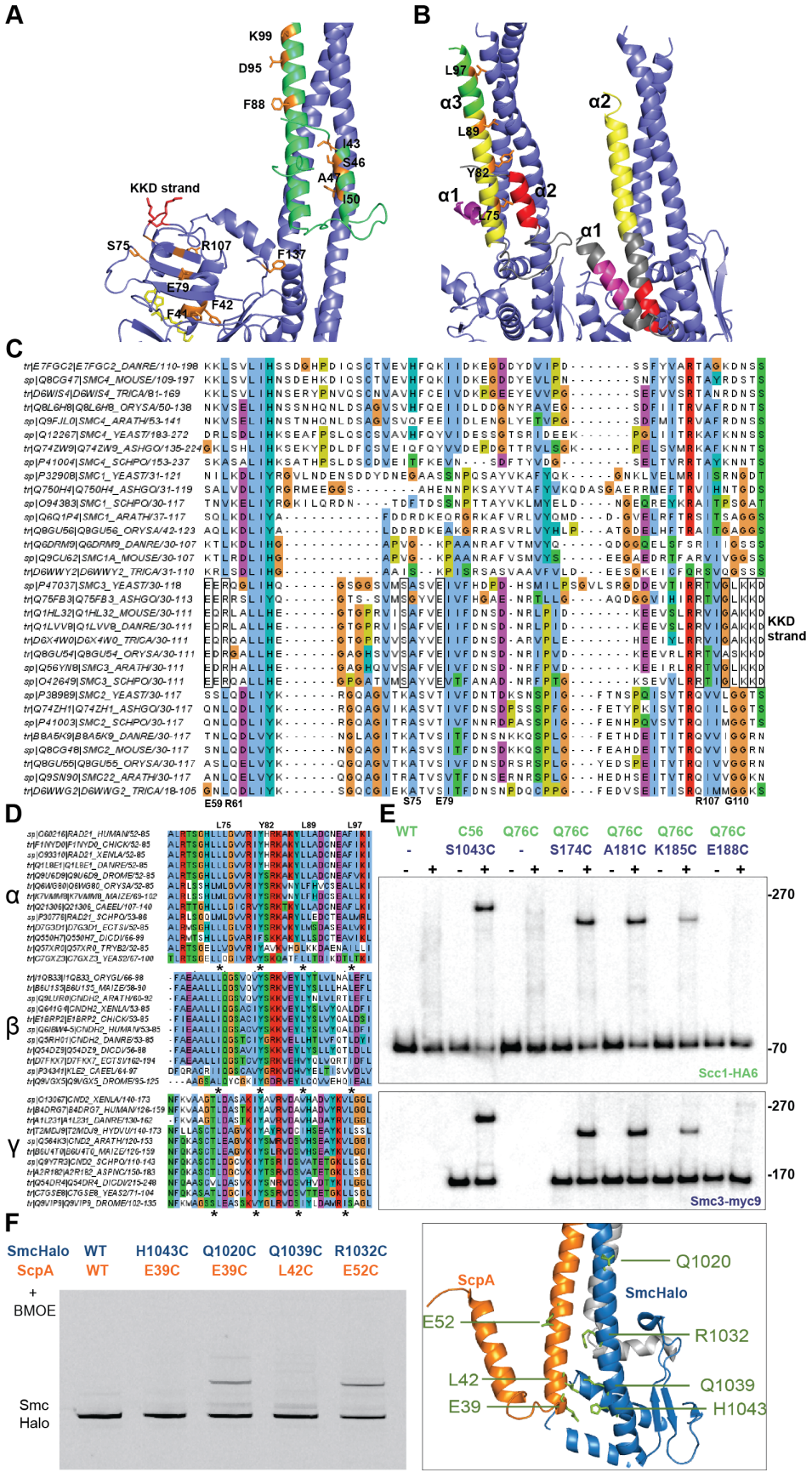
A
K99
D95
F88
I43
S46
A47
I50
KKD strand
S75
R107
F137
E79
F41
F42
B
L97
α3
L89
α2
Y82
α1
L75
α2
α1
C
KKD strand
E59 R61
S75 E79
R107 G110
D
L75 Y82 L89 L97
α
β
γ
E
WT
C56 S1043C
Q76C -
Q76C S174C
Q76C A181C
Q76C K185C
Q76C E188C
- + - + - + - + - + - + - +
-270
-70
Scc1-HA6
-270
-170
Smc3-myc9
F
SmcHalo WT H1043C Q1020C Q1039C R1032C
ScpA WT E39C E39C L42C E52C
+ BMOE
Smc
Halo
ScpA
SmcHalo
Q1020
E52
R1032
L42
Q1039
E39
H1043

Figure S4. Conservation of the Smc3 ATPase head and its interface with Scc1.

(A) The KKD strand (red) is distant from the Smc3-kleisin interface. Conserved Smc3-specific residues (F41, F42, S75, E79, R107 and F137) in the ATPase head are highlighted. Amongst these, S75R and R107I/S suppress *eco1*Δ (*15*). Scc1I43, S46, A47, and I50 are conserved and implicated in formation of the four helix bundle with Smc3's coiled coil. F88, D95 and D99, which face away from Smc3 are also highly conserved in α-kleisins.

(B) The three Scc1-N helices and corresponding residues in bacterial *B. subtilis* ScpA are colored, highlighting similarities and differences between the Smc-ScpA (*8*) and Smc3-kleisin structures.

(C) CLUSTALW alignment of Smc1, 2, 3, and 4 ATPase sequences N-terminal to Smc3's KKD strand, showing residues that are highly conserved and Smc3-specific (boxed).

(D) CLUSTALW alignment of the α3 region of α-, β-, and γ-kleisins from a diverse range of species. Residues corresponding to Scc1's L75, Y82, L89, and L97 are conserved in β- and γ- kleisins.

(E) Specificity of the thiol-specific crosslinking assay. Immuno-precipitations against Scc1-HA6 followed by in vitro cross-linking (bBBr) and Western blotting. The Scc1 Q76C substitution cross-links well with Smc3S174C and Smc3A181C, faintly with Smc3K185C and the cross-link is totally lost with Smc3E188C (Strains K18806, K19447, K19579, K19724, K19727, K19728).

(F) The Smc-ScpA complex of *B. subtilis* likely also adopts a four-helix bundle in vivo. Cysteine pairs ScpAE39C-SmcH1043C and ScpAL42C-Q1039C expected to cross link based on the *B. subtilis* structure do not cross-link using BMOE whereas the ScpAE39C-Q1020C pair designed based on the Scc1 Smc3 interface does so (not predicted to cross-link according to the *B. subtilis* structure, PDB 3ZGX). The R1032C-E52C cross-linking indicates the end of the lower part of the respective α3 helix of ScpA. The Smc-ScpA complex as determined from the crystal structure (PDB 3ZGX, panel to the right) is most likely distorted because of crystal packing artifacts.

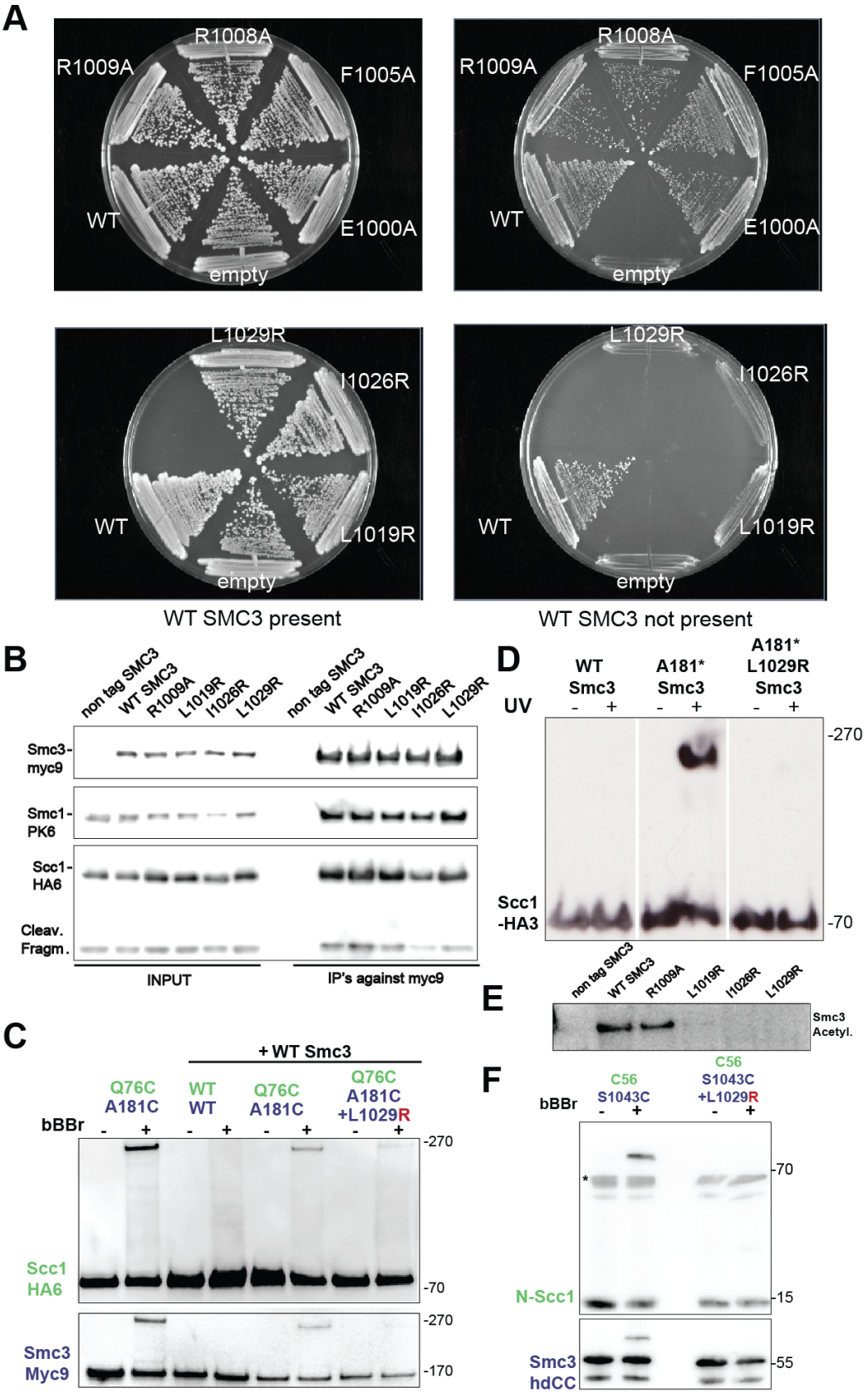
A
R1008A
R1009A
F1005A
WT
E1000A
empty
L1029R
I1026R
L1019R
WT SMC3 present
WT SMC3 not present
B
non tag SMC3
WT SMC3
R1009A
L1019R
I1026R
L1029R
Smc3-myc9
Smc1-PK6
Scc1-HA6
Cleav. Fragm.
INPUT
IP's against myc9
C
+ WT Smc3
Q76C A181C
WT WT
Q76C A181C
Q76C A181C +L1029R
bBBr
Scc1 HA6
Smc3 Myc9
-270
-70
-170
D
WT Smc3
A181* Smc3
A181* L1029R Smc3
UV
Scc1 -HA3
E
Smc3 Acetyl.
F
C56 S1043C
C56 S1043C +L1029R
N-Scc1
Smc3 hdCC
-15
-55

Figure S5. Functional analysis of the Smc3-kleisin interface.

(A) Ectopic copies of Smc3L1019R, I1026R and L1029R fail to support growth on 5-FOA plates, which select for loss of a wild type Smc3 gene carried on a centromeric plasmid. In contrast, Smc3E1000A, F1005A, R1008A, and R1009A, which are not predicted to disrupt the Smc3-kleisin interface, support growth (K23121-K23127).

(B) Immuno-precipitations of Scc1-HA6 followed by Western blotting of Scc1-HA6, Smc3-myc9 and Smc1-PK6 shows that cohesin containing Smc3L1019R, I1026R and L1029R still form complexes with Smc1 and Scc1. Scc1-HA6 presumably co-precipitates with Smc3-myc9 due to the unaffected Smc1-kleisin interface (K23147-52).

(C) Strains containing the A181C-Q76 cysteine pair, with or without Smc3L1029R, were used to immuno-precipitate Scc1-HA6 and subjected to bBBr crosslinking followed by Western blotting against Smc3-myc9 and Scc1-HA3 (K20355-57).

(D) Smc3L1029R also disrupts cross-linking induced by Smc3A181bpa. UV-irradiated cells bearing WT Smc3, Smc3A181bpa or Smc3A181bpa L1029R were used to immuno-precipitate Smc3-myc9 followed by Western blotting against Scc1-HA3 (K23153-5).

(E) Smc3 L1019R, I1026R and L1029R but not R1009A abolish K113 acetylation. Immuno-precipitations of Scc1-HA6 followed by Western blotting using anti-acetyl K113 of Smc3 (K23147-52).

(F) L1029R disrupts the Smc3-kleisin interface within complexes produced by *E. coli* in vitro but does not destroy the complex per se. Purified NScc1(6xHIS)-Smc3hdCC(StrpII) complex bearing the L1029R mutation, was precipitated using resin against Smc3Flag followed by gel filtration and then subjected to bBBr crosslinking followed by Western blotting of both Smc3hdCC and Scc1. When L1029R is present the C56-S1043C specific cross-linking is completely abolished. The asterisk denotes a non-specific band.

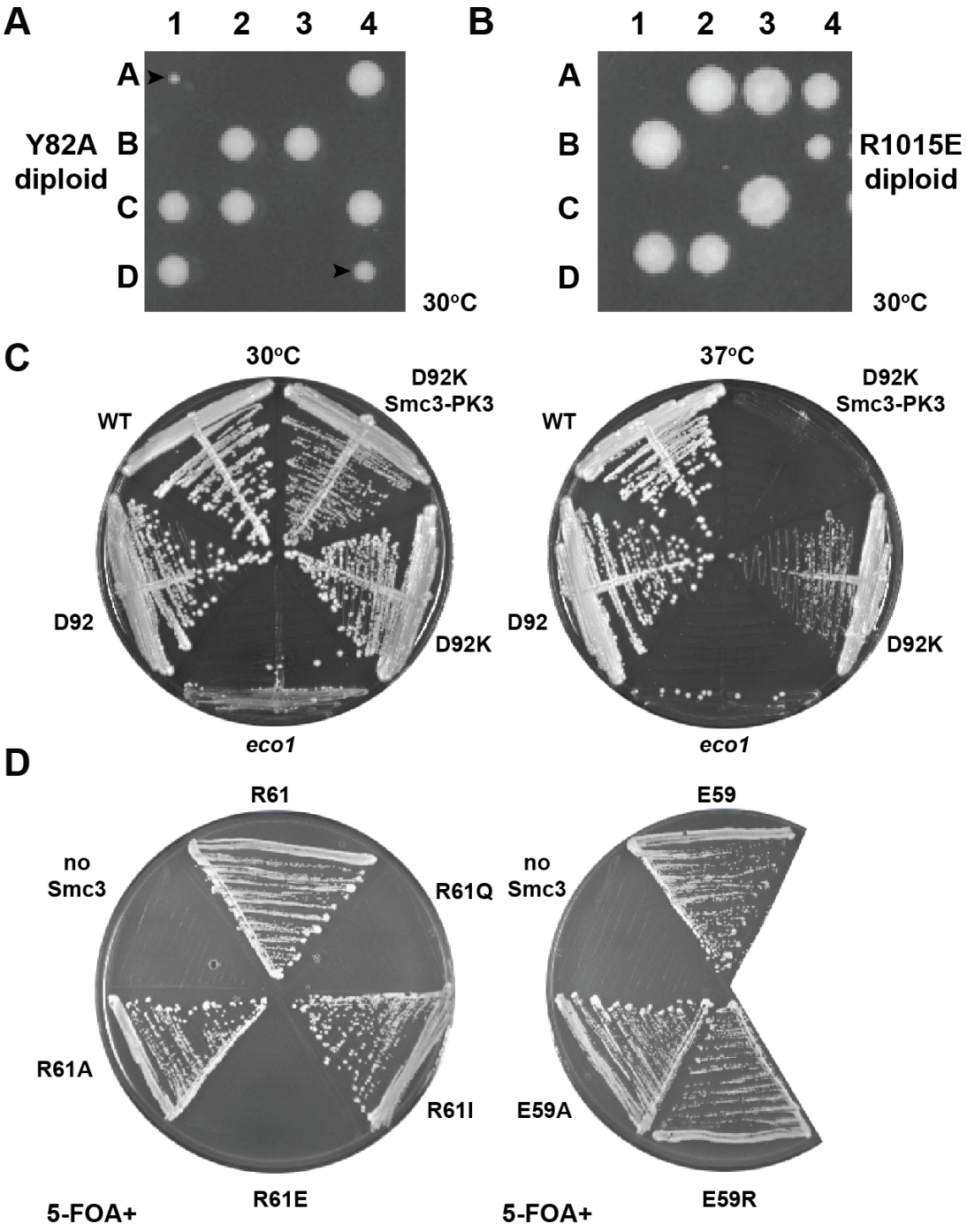
A
1 2 3 4
A
B
C
D
Y82A diploid
30°C
B
1 2 3 4
A
B
C
D
R1015E diploid
30°C
C
30°C
WT
D92K Smc3-PK3
D92
D92K
eco1
37°C
WT
D92K Smc3-PK3
D92
D92K
eco1
D
R61
no Smc3
R61Q
R61A
R61I
R61E
5-FOA+
E59
no Smc3
E59A
E59R
5-FOA+

Figure S6. Functional analysis of the Smc3-kleisin structure.

(A) Tetrad dissection of a diploid strain bearing *SCC1Δ* and an ectopic (single) copy of Scc1Y82A-HA6, at 30 ^{o}C. Scc1Y82A does not fully rescue *SCC1Δ* (white arrowheads) (K23156).

(B) Tetrad dissection of a diploid strain bearing *SMC3Δ* and an ectopic (single) copy of Smc3R1015E-myc9 at 30^{o}C (K23110). No colonies rescuing the *SMC3Δ* were recovered.

(C) Strains bearing a single copy of Scc1D92K-HA6 grow at 30 ^{o}C, poorly at 37 ^{o}C, and not at all at 37^{o}C when combined with Smc3-PK6 (K699, K23104, K16296, K23157 and K23158).

(D) Effect of substitutions close to Smc3's KKD loop. Single copy *SMC3* genes containing E59A, E59R, R61I or R61A substitutions permit growth in the absence of a WT copy of SMC3 (5-FOA counter selection). In contrast, Smc3R61Q and R61E fail to do so (K23111-23118).

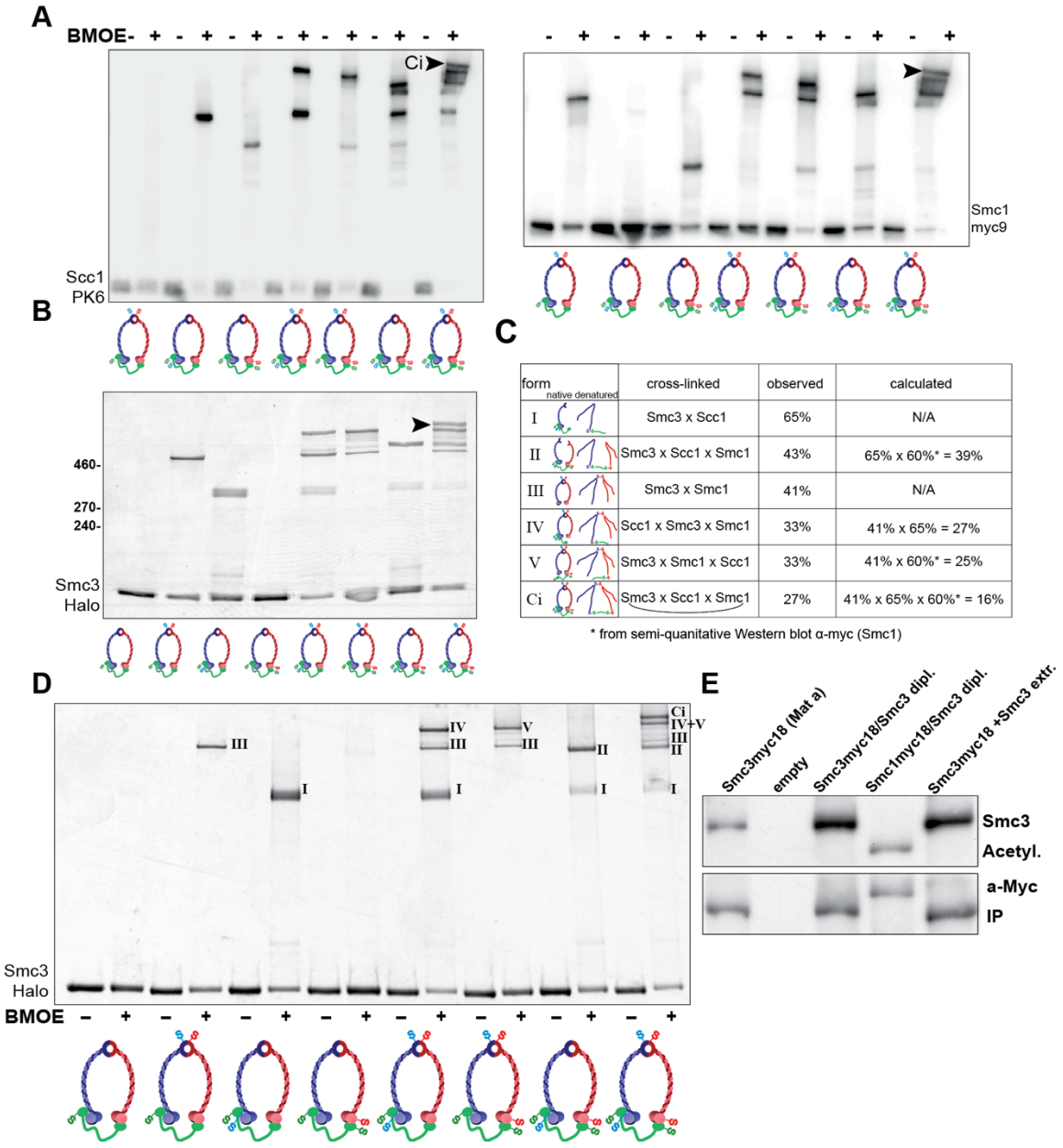
A
BMOE- + - + - + - + - + - + - +
Ci
Scc1
PK6
- + - + - + - + - + - + - +
Smc1
myc9
B
460-
270-
240-
Smc3
Halo
C
form
native denatured
cross-linked
observed
calculated
I
Smc3 x Scc1
65%
N/A
II
Smc3 x Scc1 x Smc1
43%
65% x 60%* = 39%
III
Smc3 x Smc1
41%
N/A
IV
Scc1 x Smc3 x Smc1
33%
41% x 65% = 27%
V
Smc3 x Smc1 x Scc1
33%
41% x 60%* = 25%
Ci
Smc3 x Scc1 x Smc1
27%
41% x 65% x 60%* = 16%
* from semi-quanitative Western blot α-myc (Smc1)
D
III
IV
III
V
III
II
Ci
IV+V
III
II
I
I
I
I
Smc3
Halo
BMOE – + – + – + – + – + – + – + – + – +
E
Smc3myc18 (Mat a)
empty
Smc3myc18/Smc3 dipl.
Smc1myc18/Smc3 dipl.
Smc3myc18 +Smc3 extr.
Smc3
Acetyl.
a-Myc
IP

Figure S7. Cohesin forms heterotrimeric rings.

(A) Immuno-precipitated Scc1-PK6 cohesin obtained after in vivo cross-linking using BMOE of strains K22013-K22020 was run on a 3-8 % Tris-acetate gel, proteins transferred by Western blotting and detected using anti-PK (Scc1, left) or anti-myc (Smc1, right).

(B) In vitro bBBR cross-linking and Smc3-Halo-TMR labeling after immuno-precipitation using anti-PK (strains K22013-K22020) showed the appearance of a slow migrating, high molecular weight form Ci (black arrowheads). Ci appeared only when all three interfaces contained cross-linkable cysteine pairs. Similar relative amounts of cross-linked dimers, linear trimers and circular trimer compared to in vivo cross-linking were observed.

(C and D) Observed and calculated in vivo cross-linking efficiencies for cohesin containing one, two or three cysteine pairs. Notice the difference on the resulting migrating species after denaturation, of open (V) and closed (Ci) cohesin trimers (first and second column). Cross-linking efficiencies were calculated from Halo-TMR fluorescence gels using AIDA image software and automated peak search over each lane. Efficiency of the Scc1-Smc1 crosslink was determined using semi-quantitative Western blot analysis of the anti-myc Western blot in (A) (LI-COR Odyssey FC).

(E) Acetylated cohesin contains a single Smc3 molecule. In diploid cells arrested in G2/M with nocodazole, protein encoded from the Smc3-myc18 allele fails to interact and co-precipitate with the WT acetylated Smc3 protein (K23159). Smc1-myc18 on the contrary can interact with WT acetylated Smc3 (K23160). Mixing extracts of two haploid strains bearing WT and myc-tagged Smc3 (last lane) does not lead to any exchange of subunits (K700, K700+K10905).

Supplementary Tables S1-S2

Table S1: Crystallographic data

	Smc3hd:Scc1-N native	*Smc3hd:Scc1-N SeMet*	*Smc3hd:Scc1-N(K52M) SeMet*
Components	Smc3hd: MA-2-261-SSKHPTSLVPRGS-971-1230-STRPII; Scc1-N: 1-115-HHHHHH; ATPγS	Smc3hd: MA-2-261-SSKHPTSLVPRGS-971-1230-STRPII; Scc1-N: 1-115-HHHHHH; ATPγS	Smc3hd: MA-2-261-SSKHPTSLVPRGS-971-1230-STRPII; Scc1-N: 1-(K52M)-115-HHHHHH; ATPγS
GenBank IDs	CAA89366.1; EDN60343.1	CAA89366.1; EDN60343.1	CAA89366.1; EDN60343.1
Data collection			
Beamline	Diamond I24	Diamond I02	Diamond I03
Wavelength [Å]	Se peak	Se peak	0.97934
Crystal			
Space group	I222	I222	I222
Cell [Å]	73.1, 94.8, 284.8	72.9, 92.9, 283.5	73.1, 92.0, 284.9
Scaling			
Resolution [Å]	3.3	4.0	4.2
Number of crystals	5	7	1
Completeness [%][1]	100.0 (100.0)	100.0 (100.0)	100.0 (100.0)
Multiplicity[1]	25.6 (26.6)	68.5 (65.1)	12.9 (13.4)
Ano completeness [%][1]		100.0 (100.0)	100.0 (100.0)
Ano multiplicity[1]		36.8 (33.8)	7.0 (7.1)
Ano correlation[1, 2]		0.745	0.777
$I / \sigma I$ [1]	17.7 (2.2)	18.0 (3.0)	14.0 (3.5)
R_{pim} [1]	0.022 (0.401)	0.027 (0.497)	0.039 (0.311)
CC1/2[1, 2]	0.999 (0.852)	0.998 (0.925)	0.999 (0.946)
Phasing			
Scatterer / mode		SeMet	SeMet
Number of sites		16	17
Refinement			
Model	Smc3hd: 2-81, 105-247, 975-1070, 1108-1222; 1 ATPγS; Scc1-N: 25-31, 39-102		
R / R_{free} [3]	0.274 (0.328)		
Bond length rmsd [Å]	0.011		
Bond angle rmsd [°]	1.778		
Molprobity score	3.2 (77th percentile)		
Favoured [%][4]	96.2		
Disallowed [%][4]	0.6		
PDB ID	**4UX3**		

[1] Values in parentheses refer to the highest recorded resolution shell.
[2] Correlation coefficient between half sets (CCP4 SCALA).
[3] 5 % of reflections were randomly selected before any refinement.
[4] Percentage of residues in Ramachandran plot areas (CCP4 PROCHECK).

Table S2: List of yeast strains used in this study

Strain Number	Genotype (Mutations common to all strains are not indicated but all strains are derivatives of strains K699/K700)
K699	MATa, *ade2-1*, *trp1-1*, *can1-100*, *leu2-3*,112,*his3-11,15*, URA3, GAL, psi+
K700	MATα, *ade2-1*, *trp1-1*, *can1-100*, *leu2-3*,112,*his3-11,15*, URA3, GAL, psi+
K10905	MATa, *SMC3-MYC18*::URA3
K16296	MATα , *ade2-1*, *trp1-1*, *can1-100*, *leu2-3*,112,*his3-11,15*, URA3, GAL, psi+ *eco1-1*(G211D)
K17309	MATa, GAL-*SCC1*Myc18, *scc1*::URA3, *SMC3*-PK6::KanMX4, pLH157 (TRP1+), YEpLac181-p*SCC1-SCC1*HA6 WT
K17106	MATa, GAL-*SCC1*Myc18, *scc1*::URA3, *SMC3*-PK6::KanMX4, pLH157 (TRP1+), YEpLac181-p*SCC1-SCC1*HA6 T3stop(TAG)
K17310	MATa, GAL-*SCC1*Myc18, *scc1*::URA3, *SMC3*-PK6::KanMX4, pLH157 (TRP1+), YEpLac181-p*SCC1-SCC1*HA6 W25stop(TAG)
K17311	MATa, GAL-*SCC1*Myc18, *scc1*::URA3, *SMC3*-PK6::KanMX4, pLH157 (TRP1+), YEpLac181-p*SCC1-SCC1*HA6 N5stop(TAG)
K17312	MATa, GAL-*SCC1*Myc18, *scc1*::URA3, *SMC3*-PK6::KanMX4, pLH157 (TRP1+), YEpLac181-p*SCC1-SCC1*HA6 R8stop(TAG)
K17316	MATa, GAL-*SCC1*Myc18, *scc1*::URA3, *SMC3*-PK6::KanMX4, pLH157 (TRP1+), YEpLac181-p*SCC1-SCC1*HA6 I100stop(TAG)
K17540	MATa, GAL-*SCC1*Myc18, *scc1*::URA3, *SMC3*-PK6::KanMX4, pLH157 (TRP1+), YEpLac181-p*SCC1-SCC1*HA6 P6stop(TAG)
K18806	MATa, *leu2*:*SCC1*-HA6::hphNT1::*leu2*, *scc1*::KanMX4
K19447	MATa, *leu2*:*SCC1*(Q76C)-HA6::hphNT1::*leu2*, *scc1*::KanMX4
K19579	MATa, *his3*:*SMC3*(E188C)-MYC9::natNT2::*his3*, *smc3*::HIS3MX, *leu2*:*SCC1*(Q76C)-HA6::hphNT1::*leu2*, *scc1*::KanMX4
K19724	MATa, *his3*:*SMC3*(E174C)-MYC9::natNT2::*his3*, *smc3*::HIS3MX, *leu2*:*SCC1*(Q76C)-HA6::hphNT1::*leu2*, *scc1*::KanMX4
K19727	MATa, *his3*:*SMC3*(A181C)-MYC9::natNT2::*his3*, *smc3*::HIS3MX, *leu2*:*SCC1*(Q76C)-HA6::hphNT1::*leu2*, *scc1*::KanMX4
K19728	MATa, *his3*:*SMC3*(K185C)-MYC9::natNT2::*his3*, *smc3*::HIS3MX, *leu2*:*SCC1*(Q76C)-HA6::hphNT1::*leu2*, *scc1*::KanMX4
K19732	MATa, *his3*:*SMC3*(K185C)-MYC9::natNT2::*his3*, *smc3*::HIS3MX, *leu2*:*SCC1*(R80C)-HA6::hphNT1::*leu2*, *scc1*::KanMX4
K19764	MATα, *his3*:*SMC3*(S1043C)-MYC9::natNT2::*his3*, *smc3*::HIS3MX, *leu2*:*SCC1*-HA6::hphNT1::*leu2*, *scc1*::KanMX4
K19769	MATα, *his3*:*SMC3*(S174C)-MYC9::natNT2::*his3*, *smc3*::HIS3MX, *leu2*:*SCC1*(R69C)-HA6::hphNT1::*leu2*, *scc1*::KanMX4
K19796	MATa, *his3*:*SMC3*-MYC9::natNT2::*his3*, *smc3*::HIS3MX, *leu2*:*SCC1*-HA6::hphNT1::*leu2*, *scc1*::KanMX4
K20279	MATa, *leu2*: *SMC1*(G22C,K639C)-MYC9::hphNT1::*leu2*, *SMC1*::NatMX4, *SCC1*(A547C)-PK6::KanMX4, *SMC3*(E570C,S1043C)-HA6::HIS3MX, 2.3kb TRP1-Cen4-ARS1 minichromosome
K20280	MATa, *leu2*: *SMC1*(G22C,K639C)-MYC9::hphNT1::*leu2*, *SMC1*::NatMX4, *SCC1*-PK6::KanMX4, *SMC3*(E570C,S1043C)-HA6::HIS3MX, 2.3kb TRP1-Cen4-ARS1 minichromosome
K20300	MATa, *leu2*: *SMC1*(G22C,K639C)-MYC9::hphNT1::*leu2*, *SMC1*::NatMX4, *SCC1*(C56S, A547C)-PK6::KanMX4, *SMC3*(E570C,S1043C)-HA6::HIS3MX, 2.3kb TRP1-Cen4-ARS1 minichromosome
K20355	MATa, *his3*:*SMC3*-MYC9::natNT2::*his3*, *SMC3*::HIS3MX, *leu2*:*SCC1*-HA6::hphNT1::*leu2*, *scc1*::KanMX4, *trp1*::*SMC1*::TRP1
K20356	MATa, *his3*:*SMC3*(A181C)-MYC9::natNT2::*his3*, *smc3*::HIS3MX, *leu2*:*SCC1*(Q76C)-

	HA6::hphNT1::*leu2*, *scc1*::KanMX4, *trp1*::*SMC1*::TRP1
K20357	MATa, *his3*:*SMC3*(A181C, L1029R)-MYC9::natNT2::*his3*, *smc3*::HIS3MX, *leu2*:*SCC1*(Q76C)-HA6::hphNT1::*leu2*, *scc1*::KanMX4, *trp1*::*SMC1*::TRP1
K20358	MATa, *SCC1*-PK6::KanMX4, *smc3*::HIS3MX, pLH157, YCpLac33-*SMC3*-MYC9, YEpLac181-*SMC3*-HA3
K20359	MATa, *SCC1*-PK6::KanMX4, *smc3*::HIS3MX, pLH157, YCpLac33-*smc3*-MYC9, YEpLac181-*smc3*(A181*amber*)-HA3
K20360	MATa, *SCC1*-PK6::KanMX4, *smc3*::HIS3MX, pLH157, YCpLac33-*SMC3*-MYC9, YEpLac181-*SMC3*(K185*amber*)-HA3
K20361	MATa, *SCC1*-PK6::KanMX4, *smc3*::HIS3MX, pLH157, YCpLac33-*SMC3*-MYC9, YEpLac181-*SMC3*(K206*amber*)-HA3
K20362	MATa, *SCC1*-PK6::KanMX4, *smc3*::HIS3MX, pLH157, YCpLac33-*SMC3*-MYC9, YEpLac181-*SMC3*(K1018*amber*)-HA3
K20363	MATa, *SCC1*-PK6::KanMX4, *smc3*::HIS3MX, pLH157, YCpLac33-*SMC3*-MYC9, YEpLac181-*SMC3*(A1040*amber*)-HA3
K20364	MATa, *SCC1*-PK6::KanMX4, *smc3*::HIS3MX, pLH157, YCpLac33-*SMC3*-MYC9, YEpLac181-*SMC3*(E1050*amber*)-HA3
K20366	MATa, *smc3*::HIS3MX, Nmyc9-*SCC1*(Met1Ile, Met30Ile), YEpLac181-*SMC3*-HA3, pLH157
K20367	MATa, *smc3*::HIS3MX, Nmyc9-*SCC1*(Met1Ile, Met30Ile), YEpLac181-*SMC3*(A181*amber*)-HA3, pLH157
K22013	MATα, *leu2*:*SMC1*-MYC9::hphNT1::*leu2*, *SMC1*::NatMX4, *SCC1*-PK6::KanMX4, *SMC3*-Halo::ADE2
K22014	MATα, *leu2*:*SMC1*(K639C)-MYC9::hphNT1::*leu2*, *SMC1*::NatMX4, *SCC1*-PK6::KanMX4, *SMC3*(E570C)-Halo::ADE2
K22015	MATa, *leu2*:*SMC1*-MYC9::hphNT1::*leu2*, *SMC1*::NatMX4, *SCC1*-PK6::KanMX4, *SMC3*(S1043C)-Halo::ADE2
K22016	MATα, *leu2*:*SMC1*(K639C)-MYC9::hphNT1::*leu2*, *SMC1*::NatMX4, *SCC1*-PK6::KanMX4, *SMC3*(E570C,S1043C)-Halo::ADE2
K22017	MATα, *leu2*:*SMC1*(G22C)-MYC9::hphNT1::*leu2*, *SMC1*::NatMX4, *SCC1*(A547C)-PK6::KanMX4, *SMC3*-Halo::ADE2
K22018	MATa, *leu2*:*SMC1*(G22C,K639C)-MYC9::hphNT1::*leu2*, *SMC1*::NatMX4, *SCC1*(A547C)-PK6::KanMX4, *SMC3*(E570C)-Halo::ADE2
K22019	MATa, *leu2*:*SMC1*(G22C,K639C)-MYC9::hphNT1::*leu2*, *SMC1*::NatMX4, *SCC1*(A547C)-PK6::KanMX4, *SMC3*(E570C,S1043C)-Halo::ADE2
K22020	MATa, *leu2*:*SMC1*(G22C)-MYC9::hphNT1::*leu2*, *SMC1*::NatMX4, *SCC1*(A547C)-PK6::KanMX4, *SMC3*(S1043C))-Halo::ADE2
K22590	MATa,/α, *leu2*:*SMC1*(G22C,K639C)-MYC9::hphNT1::*leu2*/ *leu2*:*SMC1*(G22C,K639C)-MYC9::hphNT1::*leu2*, *SMC1*::NatMX4/*SMC1*::NatMX4, *SCC1*(A547C)-PK6::KanMX4/*SCC1*(A547C)-PK6::KanMX4, *SMC3*(E570C,S1043C)-Halo::ADE2/*SMC3*(E570C,S1043C)-HA6::HIS3MX
K23102	MATa, *his3*:*SMC3*(K1032C)-MYC9::natNT2::*his3*, *SMC3*::HIS3MX, *leu2*:*SCC1*(C56S K48C)-HA6::hphNT1::*leu2*, *scc1*::KanMX4
K23103	MATa, *his3*:*SMC3*(F1005C)-MYC9::natNT2::*his3*, *SMC3*::HIS3MX, *leu2*:*SCC1*(I100C)-HA6::hphNT1::*leu2*, *scc1*::KanMX4
K23104	MATa, *leu2*:*SCC1*-HA6::hphNT1::*leu2*, *scc1*::KanMX4
K23105	MATa, *leu2*:*SCC1*(Y82A)-HA6::hphNT1::*leu2*, *scc1*::KanMX4, spore 12D
K23106	MATa, *leu2*:*SCC1*(Y82A)-HA6::hphNT1::*leu2*, *scc1*::KanMX4, spore 5D
K23107	MATa,/α *leu2*::*SMC3*GFP::LEU2 Mtw1-RFP:KanMX4 *SMC1*myc9::URA3 *leu2*::*SCC1*HA6:hphNT1/*leu2*::*SMC3*GFP::LEU2 Mtw1-RFP:KanMX4 *SMC1*myc9::URA3 *leu2*::*SCC1*HA6::hphNT1
K23108	MATa,/α *leu2*::*SMC3*(L1029R)GFP::LEU2 Mtw1-RFP:KanMX4 *SMC1*myc9::URA3 *leu2*::*SCC1*HA6:hphNT1/*leu2*::*SMC3*(L1029R)GFP::LEU2 Mtw1-RFP:KanMX4 *SMC1*myc9::URA3 *leu2*::*SCC1*HA6::hphNT1
K23109	MATa,/α *leu2*::*SMC3*(R61Q)GFP::LEU2 Mtw1-RFP:KanMX4 *SMC1*myc9::URA3

	leu2::*SCC1*HA6:hphNT1/*leu2*::*SMC3*(R61Q)GFP::LEU2 Mtw1- RFP:KanMX4 *SMC1*myc9::URA3 *leu2*::*SCC1*HA6::hphNT1RFP:KanMX4 *SMC1*myc9::URA3 *leu2*::*SCC1*HA6::hphNT1
K23110	MATa,/α, *his3*:*SMC3*(R1015E)-MYC9::natNT2::*his3*, *SMC3*::HIS3MX
K23111	MATa,*smc3*::hphNT1 *his3*:natNT2::*his3* + YCpLac33-*SMC3*myc9
K23112	MATa,*smc3*::hphNT1 *his3*:*SMC3*-MYC9:natNT2::*his3*,YCpLac33-*SMC3*myc9
K23113	MATa, *smc3*::hphNT1 *his3*:*SMC3*(R61I)-MYC9::natNT2::*his3*,YCpLac33-*SMC3*myc9
K23114	MATa, *smc3*::hphNT1 *his3*:*SMC3*(R61Q)-MYC9::natNT2::*his3*,YCpLac33-*SMC3*myc9
K23115	MATa, *smc3*::hphNT1 *his3*:*SMC3*(R61A)-MYC9::natNT2::*his3*,YCpLac33-*SMC3*myc9
K23116	MATa, *smc3*::hphNT1 *his3*:*SMC3*(R61E)-MYC9::natNT2::*his3*,YCpLac33-*SMC3*myc9
K23117	MATa, *smc3*::hphNT1 *his3*:*SMC3*(E59A)-MYC9::natNT2::*his3*, YCpLac33-*SMC3*myc9
K23118	MATa, *smc3*::hphNT1 *his3*:*SMC3*(E59R)-MYC9::natNT2::*his3*,YCpLac33-*SMC3*myc9
K23119	MATa, *scc1*::NatMX4 , *leu2*:*SCC1*R69E)-HA6::hphNT1::*leu2*
K23120	MATa, *scc1*::NatMX4 , *leu2*:*SCC1*(R69A)-HA6::hphNT1::*leu2*
K23121	MATa, *SMC3*::hphNT1 *his3*:*SMC3*(E1000A)-MYC9::natNT2::*his3*,YCpLac33-*SMC3*myc9
K23122	MATa, *smc3*::hphNT1 *his3*:*SMC3*(F1005A)-MYC9::natNT2::*his3*,YCpLac33-*SMC3*myc9
K23123	MATa, *smc3*::hphNatMX4 *his3*:*SMC3*(R1008A)-MYC9::natNT2::*his3*,YCpLac33-*SMC3*myc9
K23124	MATa, *smc3*::hphMX*4 his3*:*SMC3*(R1009A)-MYC9::natNT2::*his3*,YCpLac33-*SMC3*myc9
K23125	MATa, *smc3*::hphMX4 *his3*:*SMC3*(L1029R)-MYC9::natNT2::*his3*,YCpLac33-*SMC3*myc9
K23126	MATa, *smc3*::hphMX*4 his3*:*SMC3*(I1026R)-MYC9::natNT2::*his3*,YCpLac33-*SMC3*myc9
K23127	MATa, *smc3*::hphMX4 *his3*:*SMC3*(L1029R)-MYC9::natNT2::*his3*,YCpLac33-*SMC3*myc9
K23128	MATa, *his3*:*SMC3*(S1043C)-MYC9::natNT2::*his3*, *smc3*::HIS3MX, *leu2*:*SCC1*-HA6::hphNT1::*leu2*, *scc1*::KanMX4, *trp1*::*SMC1*::TRP1
K23129	MATa, *his3*:*SMC3*(S1043C,L1029R)-MYC9::natNT2::*his3*, *smc3*::HIS3MX, *leu2*:*SCC1*-HA6::hphNT1::*leu2*, *scc1*::KanMX4, *trp1*::*SMC1*::TRP1
K23130	MATa, *smc3*::HIS3MX *his3*:*SMC3*(S1043C)-MYC9::natNT2::*his3*, ,*leu2*:*SCC1*-HA6::hphNT1::*leu2*
K23131	MATa, *smc3*::HIS3MX *his3*:*SMC3*(S1043C)-MYC9::natNT2::*his3*, ,*leu2*:*SCC1*(L89K)-HA6::hphNT1::*leu2*
K23132	MATa,/α *his3*:*SMC3*hphMX4, , *his3*:*SMC3*(K206E)-MYC9::natNT2::*his3*
K23133	MATa,/α *his3*:*SMC3*hphMX4, , *his3*:*SMC3*(E216A)-MYC9::natNT2::*his3*
K23134	MATa, *smc3*::hphMX4 *his3*:*SMC3*(K996A)-MYC9::natNT2::*his3*,YCpLac33-*SMC3*myc9
K23135	MATa, *smc3*::hphMX4 *his3*:*SMC3*(K996D)-MYC9::natNT2::*his3*,YCpLac33-*SMC3*myc9
K23136	MATa, *scc1*::NatMX4 , *leu2*:*SCC1*(Y82I)-HA6::hphNT1::leu2, *scc1*::KanMX4
K23137	MATa, *scc1*::NatMX4 , *leu2*:*SCC1*(Y82F)-HA6::hphNT1::leu2, *scc1*::KanMX4
K23138	MATa, *scc1*::NatMX4 , *leu2*::hphNT1::leu2, YCpLac33-*pSCC1-SCC1*
K23139	MATa, *scc1*::NatMX4 , *leu2*:: *SCC1*-HA6hphNT1::leu2, YCpLac33-*pSCC1-SCC1*
K23140	MATa, *scc1*::NatMX4 , *leu2*:*SCC1*(D95K)-HA6::hphNT1::leu2, YCpLac33-*pSCC1-SCC1*
K23141	MATa, *scc1*::NatMX4 , *leu2*:*SCC1*(K99D)-HA6::hphNT1::leu2, YCpLac33-*pSCC1-SCC1*
K23142	MATa, *scc1*::NatMX4 , *leu2*:*SCC1*(K99A)-HA6::hphNT1::leu2, YCpLac33-*pSCC1-SCC1*
K23143	MATa,/α *scc1*::NatMX4 , *leu2*:*SCC1*(D95A,K99A)-HA6::hphNT1::*leu2, SMC3*-PK6
K23146	MATa, *his3*:*SMC3*-MYC9::natNT2::*his3*, *smc3*::HIS3MX, *leu2*:*SCC1*-

	HA6::hphNT1::*leu2*, *scc1*::KanMX4, *trp1*::*SMC1*::TRP1
K23147	MATa, *SCC1*-HA6::HIS3MX, *SMC1*-PK6::KanMX6, *his3*::natNT2::*his3*
K23148	MATa, *SCC1*-HA6::HIS3MX, *SMC1*-PK6::KanMX6, *his3*:SMC3-MYC9:natNT2::*his3*
K23149	MATa, *SCC1*-HA6::HIS3MX, *SMC1*-PK6::KanMX6, *his3*:*SMC3*(R1009A)-MYC9::natNT2::*his3*
K23150	MATa, *SCC1*-HA6::HIS3MX, *SMC1*-PK6::KanMX6, *his3*:*SMC3*(L1019R)-MYC9::natNT2::*his3*
K23151	MATa, *SCC1*-HA6::HIS3MX, *SMC1*-PK6::KanMX6, *his3*:*SMC3*(I1026R)-MYC9::natNT2::*his3*
K23152	MATa, *SCC1*-HA6::HIS3MX, *SMC1*-PK6::KanMX6, *his3*:*SMC3*(L1029R)-MYC9::natNT2::*his3*
K23153	MATa, *SCC1*-PK6::KanMX4, pLH157, YEpLac181-*SMC3*-HA3
K23154	MATa, *SCC1*-PK6::KanMX4, pLH157, YEpLac181-*SMC3*A181*amber*-HA3
K23155	MATa, *SCC1*-PK6::KanMX4, pLH157, YEpLac181-*SMC3*A181*amber*,L1029R-HA3
K23156	MATa,/α *scc1*::NatMX4 , *leu2*:*SCC1*(Y82A)-HA6::hphNT1::*leu2, SMC3*-PK6::KanMX6
K23157	MATa, *scc1*::NatMX4 , *leu2*:*SCC1*(D92K)-HA6::hphNT1::*leu2*
K23158	MATa, *scc1*::NatMX4 , *leu2*:*SCC1*(D92K)-HA6::hphNT1::*leu2, SMC3*-PK6::KanMX6
K23159	MATa,/α *SMC3-MYC18*::URA3
K23160	MATa,/α *SMC1-MYC18*::URA3

References and Notes

1. J. M. Peters, A. Tedeschi, J. Schmitz, The cohesin complex and its roles in chromosome biology. *Genes Dev.* **22**, 3089–3114 (2008). Medline doi:10.1101/gad.1724308

2. K. Nasmyth, Cohesin: A catenase with separate entry and exit gates? *Nat. Cell Biol.* **13**, 1170–1177 (2011). Medline doi:10.1038/ncb2349

3. S. Gruber, C. H. Haering, K. Nasmyth, Chromosomal cohesin forms a ring. *Cell* **112**, 765–777 (2003). Medline doi:10.1016/S0092-8674(03)00162-4

4. C. H. Haering, J. Löwe, A. Hochwagen, K. Nasmyth, Molecular architecture of SMC proteins and the yeast cohesin complex. *Mol. Cell* **9**, 773–788 (2002). Medline doi:10.1016/S1097-2765(02)00515-4

5. S. Gruber, P. Arumugam, Y. Katou, D. Kuglitsch, W. Helmhart, K. Shirahige, K. Nasmyth, Evidence that loading of cohesin onto chromosomes involves opening of its SMC hinge. *Cell* **127**, 523–537 (2006). Medline doi:10.1016/j.cell.2006.08.048

6. K. L. Chan, M. B. Roig, B. Hu, F. Beckouët, J. Metson, K. Nasmyth, Cohesin's DNA exit gate is distinct from its entrance gate and is regulated by acetylation. *Cell* **150**, 961–974 (2012). Medline doi:10.1016/j.cell.2012.07.028

7. K. L. Chan, T. Gligoris, W. Upcher, Y. Kato, K. Shirahige, K. Nasmyth, F. Beckouët, Pds5 promotes and protects cohesin acetylation. *Proc. Natl. Acad. Sci. U.S.A.* **110**, 13020–13025 (2013). Medline doi:10.1073/pnas.1306900110

8. F. Bürmann, H. C. Shin, J. Basquin, Y. M. Soh, V. Giménez-Oya, Y. G. Kim, B. H. Oh, S. Gruber, An asymmetric SMC-kleisin bridge in prokaryotic condensin. *Nat. Struct. Mol. Biol.* **20**, 371–379 (2013). Medline doi:10.1038/nsmb.2488

9. C. H. Haering, A. M. Farcas, P. Arumugam, J. Metson, K. Nasmyth, The cohesin ring concatenates sister DNA molecules. *Nature* **454**, 297–301 (2008). Medline doi:10.1038/nature07098

10. A. Schleiffer, S. Kaitna, S. Maurer-Stroh, M. Glotzer, K. Nasmyth, F. Eisenhaber, Kleisins: A superfamily of bacterial and eukaryotic SMC protein partners. *Mol. Cell* **11**, 571–575 (2003). Medline doi:10.1016/S1097-2765(03)00108-4

11. P. Arumugam, T. Nishino, C. H. Haering, S. Gruber, K. Nasmyth, Cohesin's ATPase activity is stimulated by the C-terminal Winged-Helix domain of its kleisin subunit. *Curr. Biol.* **16**, 1998–2008 (2006). Medline doi:10.1016/j.cub.2006.09.002

12. B. Hu, T. Itoh, A. Mishra, Y. Katoh, K. L. Chan, W. Upcher, C. Godlee, M. B. Roig, K. Shirahige, K. Nasmyth, ATP hydrolysis is required for relocating cohesin from sites occupied by its Scc2/4 loading complex. *Curr. Biol.* **21**, 12–24 (2011). Medline doi:10.1016/j.cub.2010.12.004

13. E. Unal, J. M. Heidinger-Pauli, W. Kim, V. Guacci, I. Onn, S. P. Gygi, D. E. Koshland, A molecular determinant for the establishment of sister chromatid cohesion. *Science* **321**, 566–569 (2008). Medline doi:10.1126/science.1157880

14. T. Rolef Ben-Shahar, S. Heeger, C. Lehane, P. East, H. Flynn, M. Skehel, F. Uhlmann, Eco1-dependent cohesin acetylation during establishment of sister chromatid cohesion. *Science* **321**, 563–566 (2008). Medline doi:10.1126/science.1157774

15. B. D. Rowland, M. B. Roig, T. Nishino, A. Kurze, P. Uluocak, A. Mishra, F. Beckouët, P. Underwood, J. Metson, R. Imre, K. Mechtler, V. L. Katis, K. Nasmyth, Building sister chromatid cohesion: Smc3 acetylation counteracts an antiestablishment activity. *Mol. Cell* **33**, 763–774 (2009). Medline doi:10.1016/j.molcel.2009.02.028

16. F. Beckouët, B. Hu, M. B. Roig, T. Sutani, M. Komata, P. Uluocak, V. L. Katis, K. Shirahige, K. Nasmyth, An Smc3 acetylation cycle is essential for establishment of sister chromatid cohesion. *Mol. Cell* **39**, 689–699 (2010). Medline doi:10.1016/j.molcel.2010.08.008

17. T. Sutani, T. Kawaguchi, R. Kanno, T. Itoh, K. Shirahige, Budding yeast Wpl1(Rad61)-Pds5 complex counteracts sister chromatid cohesion-establishing reaction. *Curr. Biol.* **19**, 492–497 (2009). Medline doi:10.1016/j.cub.2009.01.062

18. C. E. Huang, M. Milutinovich, D. Koshland, Rings, bracelet or snaps: Fashionable alternatives for Smc complexes. *Philos. Trans. R. Soc. London B Biol. Sci.* **360**, 537–542 (2005). Medline doi:10.1098/rstb.2004.1609

19. D. Ivanov, K. Nasmyth, A physical assay for sister chromatid cohesion in vitro. *Mol. Cell* **27**, 300–310 (2007). Medline doi:10.1016/j.molcel.2007.07.002

20. C. H. Haering, D. Schoffnegger, T. Nishino, W. Helmhart, K. Nasmyth, J. Löwe, Structure and stability of cohesin's Smc1-kleisin interaction. *Mol. Cell* **15**, 951–964 (2004). Medline doi:10.1016/j.molcel.2004.08.030

21. A. Kurze, K. A. Michie, S. E. Dixon, A. Mishra, T. Itoh, S. Khalid, L. Strmecki, K. Shirahige, C. H. Haering, J. Löwe, K. Nasmyth, A positively charged channel within the Smc1/Smc3 hinge required for sister chromatid cohesion. *EMBO J.* **30**, 364–378 (2011). Medline doi:10.1038/emboj.2010.315

22. F. Uhlmann, F. Lottspeich, K. Nasmyth, Sister-chromatid separation at anaphase onset is promoted by cleavage of the cohesin subunit Scc1. *Nature* **400**, 37–42 (1999). Medline doi:10.1038/21831

23. S. B. Buonomo, R. K. Clyne, J. Fuchs, J. Loidl, F. Uhlmann, K. Nasmyth, Disjunction of homologous chromosomes in meiosis I depends on proteolytic cleavage of the meiotic cohesin Rec8 by separin. *Cell* **103**, 387–398 (2000). Medline doi:10.1016/S0092-8674(00)00131-8

24. A. Losada, M. Hirano, T. Hirano, Identification of Xenopus SMC protein complexes required for sister chromatid cohesion. *Genes Dev.* **12**, 1986–1997 (1998). Medline doi:10.1101/gad.12.13.1986

25. I. Sumara, E. Vorlaufer, C. Gieffers, B. H. Peters, J.-M. Peters, Characterization of vertebrate cohesin complexes and their regulation in prophase. *J. Cell Biol.* **151**, 749–762 (2000). Medline doi:10.1083/jcb.151.4.749

26. R. Gandhi, P. J. Gillespie, T. Hirano, Human Wapl is a cohesin-binding protein that promotes sister-chromatid resolution in mitotic prophase. *Curr. Biol.* **16**, 2406–2417 (2006). Medline doi:10.1016/j.cub.2006.10.061

27. S. Kueng, B. Hegemann, B. H. Peters, J. J. Lipp, A. Schleiffer, K. Mechtler, J. M. Peters, Wapl controls the dynamic association of cohesin with chromatin. *Cell* **127**, 955–967 (2006). Medline doi:10.1016/j.cell.2006.09.040

28. M. B. Roig , J. Löwe , K. L. Chan, F. Beckouët, J. Metson, K. Nasmyth, Structure and function of cohesin's Scc3/SA regulatory subunit. *FEBS Lett.* **16**, 3692–3702 (2014).

29. H. T. Chen, L. Warfield, S. Hahn, The positions of TFIIF and TFIIE in the RNA polymerase II transcription preinitiation complex. *Nat. Struct. Mol. Biol.* **14**, 696–703 (2007). Medline doi:10.1038/nsmb1272

30. A. M. Farcas, P. Uluocak, W. Helmhart, K. Nasmyth, Cohesin’s concatenation of sister DNAs maintains their intertwining. *Mol. Cell* **44**, 97–107 (2011). Medline doi:10.1016/j.molcel.2011.07.034

31. D. Stock, O. Perisic, J. Löwe, Robotic nanolitre protein crystallisation at the MRC Laboratory of Molecular Biology. *Prog. Biophys. Mol. Biol.* **88**, 311–327 (2005). Medline doi:10.1016/j.pbiomolbio.2004.07.009

32. W. Kabsch, Integration, scaling, space-group assignment and post-refinement. *Acta Crystallogr. D Biol. Crystallogr.* **66**, 133–144 (2010). Medline doi:10.1107/S0907444909047374

33. M. D. Winn, C. C. Ballard, K. D. Cowtan, E. J. Dodson, P. Emsley, P. R. Evans, R. M. Keegan, E. B. Krissinel, A. G. Leslie, A. McCoy, S. J. McNicholas, G. N. Murshudov, N. S. Pannu, E. A. Potterton, H. R. Powell, R. J. Read, A. Vagin, K. S. Wilson, Overview of the CCP4 suite and current developments. *Acta Crystallogr. D Biol. Crystallogr.* **67**, 235–242 (2011). Medline doi:10.1107/S0907444910045749

34. A. J. McCoy, R. W. Grosse-Kunstleve, P. D. Adams, M. D. Winn, L. C. Storoni, R. J. Read, Phaser crystallographic software. *J. Appl. Cryst.* **40**, 658–674 (2007). Medline doi:10.1107/S0021889807021206

35. D. Turk, MAIN software for density averaging, model building, structure refinement and validation. *Acta Crystallogr. D Biol. Crystallogr.* **69**, 1342–1357 (2013). Medline doi:10.1107/S0907444913008408

36. G. N. Murshudov, A. A. Vagin, E. J. Dodson, Refinement of macromolecular structures by the maximum-likelihood method. *Acta Crystallogr. D Biol. Crystallogr.* **53**, 240–255 (1997). Medline doi:10.1107/S0907444996012255